THE JOURNAL OF PHYSICAL CHEMISTRY C

Feature Article

Cite This: J. Phys. Chem. C 2018, 122, 10659−10674

pubs.acs.org/JPCC

Carrier Dynamics, Optical Gain, and Lasing with Colloidal Quantum Wells

Matthew Pelton*

Department of Physics, University of Maryland Baltimore County, Baltimore, Maryland 21250, United States

ABSTRACT: The most recent class of semiconductor nanocrystal to be synthesized colloidally is the quantum well, in which carriers are confined quantum mechanically in only one dimension. Electrons and holes in colloidal quantum wells undergo different dynamics than in either colloidal quantum dots or epitaxially grown quantum wells, providing new opportunities for applications. The opportunities presented by cadmium chalcogenide nanoplatelets are particularly exciting, because they can be grown with control over their thickness down to the single atomic layer and with all nanoplatelets in an ensemble having the same thickness. This Feature Article reviews the relaxation and recombination dynamics of electrons and holes, which are tightly bound into excitons, in nanoplatelets. These dynamics are favorable for optical gain and lasing, and this Article reviews the progress that has been made toward practical realization of nanoplatelet lasers, including the demonstration of low thresholds for room-temperature gain and lasing. Looking forward, the engineering of nanoplatelet heterostructures provides new opportunities to control carrier dynamics, opening up in particular the possibility of observing strong multiexcitonic effects at room temperature.

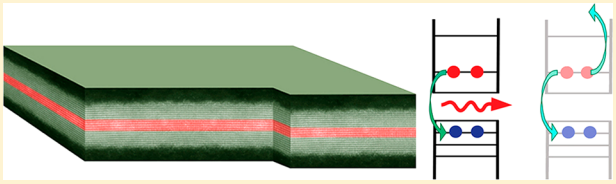

1. INTRODUCTION

Since the first demonstrations that the energy states of carriers in semiconductor nanocrystals are quantized,[1,2] the nanocrystals have been studied for their tunable photophysical properties and their potential applications. A wide range of applications have been investigated,[3] such as nanocrystal-based field-effect transistors and solar cells,[4] but the most intensively studied involve using the nanocrystals as light-emitting materials.[5] Light-emitting applications were enabled by the development of robust methods to synthesize monodisperse, luminescent nanocrystals as colloids in organic solvents[6] and the extension of these methods to produce highly luminescent core/shell nanocrystals.[7] The nanocrystals synthesized by these methods, and the majority of the nanocrystals studied since then, are quasi-spherical particles of II−VI semiconductors, most commonly CdSe, in which carriers are confined quantum mechanically in all three dimensions. These spherical nanocrystals, or quantum dots (QDs), have several advantages over other solution-processable light emitters, including the ability to broadly tune emission wavelength by changing nanocrystal dimension and composition, high photoluminescence quantum yield (QY), and high photostability. Because of these advantages, colloidal QDs have found laboratory applications in labeling for fluorescence microscopy,[8] commercial applications in displays,[9] and emerging applications in light-emitting diodes (LEDs).[10,11]

These successes make it natural to consider colloidal QDs as gain materials for lasers. Their wavelength tunability means a broad range of laser frequencies could be accessed, and their solution processability means that lasers could be integrated onto arbitrary substrates, including CMOS-compatible substrates, flexible substrates, and lab-on-a chip platforms. However, achieving practical lasing with colloidal QDs has proved challenging. Early attempts to demonstrate optical gain and stimulated emission resulted in high threshold energy densities,[12] and until recently, lasing was observed only under pulsed excitation and generally at low temperature.[13,14] The suitability of QDs for displays and LEDs, and the challenges involved in using them in lasers, ultimately arise from the different dynamical processes that electrons and holes in the materials undergo, as illustrated in Figure 1.

Nearly all applications of QDs as light emitters involve, as a first step, exciting electrons and holes into high-lying states in the conduction and valence bands, either optically or electrically. A high luminescence QY is achieved if the carriers relax from the high-energy states to the lowest-energy states in the bands through a series of discrete intermediate states[15] and subsequently recombine radiatively by emitting a photon. Relaxation competes with carrier trapping at defect sites and with carrier ejection, or ionization, from the QD. Radiative recombination competes with nonradiative recombination and carrier trapping. Achieving efficient light emission is thus a matter of ensuring that the rates of desired relaxation and radiative recombination processes outstrip the rates of competing processes.

Trapping of band-edge carriers and nonradiative recombination are the most significant factors affecting luminescence QY of II−VI QDs, because intraband relaxation rates in the QDs are generally much faster than interband recombination rates. It was originally hypothesized that intraband relaxation in QDs would be slow: in bulk semiconductors, relaxation occurs primarily through emission of acoustic phonons, but the energy

Received: December 22, 2017
Revised: February 5, 2018
Published: February 7, 2018

DOI: 10.1021/acs.jpcc.7b12629
J. Phys. Chem. C 2018, 122, 10659−10674

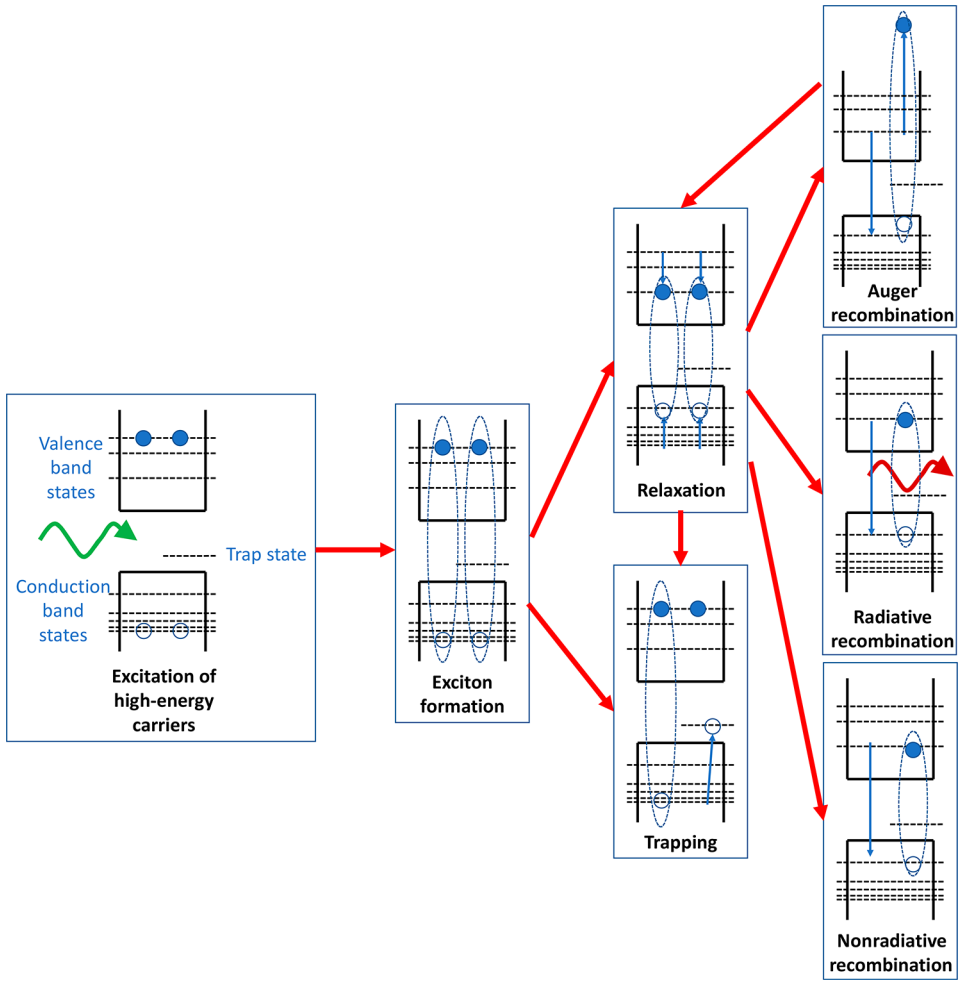

Figure 1. Schematic of key dynamical processes in semiconductor nanocrystals. Filled circles represent electrons, and hollow circles represent holes. The representation is illustrative, rather than quantitative; in particular, the energy structure of the nanocrystals is simplified, and processes are illustrated as occurring sequentially although they can occur simultaneously.

separation between confined states in QDs does not match available phonon energies. However, this predicted "phonon bottleneck" is usually not observed, because several new relaxation mechanisms become available in QDs, including an Auger-like process where an electron relaxes by transferring its energy to a hole,[16,17] coupling of carriers to defect states,[18] and coupling of carriers to vibrational modes in capping molecules.[19,20] As a result, relaxation typically occurs on picosecond time scales.[21]

Radiative recombination in II–VI QDs, by contrast, occurs on time scales of the order of 10 ns at room temperature, significantly slower than in bulk semiconductors. This slow recombination is a consequence of the fact that the lowest-energy electron–hole state in the QDs is a "dark exciton" with low oscillator strength, due to strong electron–hole exchange interaction in the QD.[22] At room temperature, recombination occurs primarily through the fraction of the population that is thermally excited into a higher-lying "bright exciton" state.[23] High luminescence QY thus requires that trapping and nonradiative recombination rates are much slower than the already slow radiative recombination rate, and a major focus of efforts to improve QY has been the elimination of defects that are responsible for trapping. Isolating carriers, especially holes, from surface trap states by growing a shell of a high-bandgap semiconductor significantly improves QY,[7,24] with recent syntheses giving QYs in solution of 97% or better.[25]

However, these high QYs apply only for low densities of excitons in the QDs, corresponding to the low excitation levels that are typically experienced in displays and LEDs. Lasers, by contrast, require high exciton densities to achieve population inversion and gain. At these high excitation levels, fast multiexciton nonradiative recombination processes occur, leading to fast optical gain decay.[5] Specifically, biexcitons in QDs undergo rapid Auger recombination, where one exciton recombines and its energy is transferred to one of the carriers in the other exciton, promoting it to a higher-energy level in its band.[26] This process is slow in bulk semiconductors because of the need to conserve momentum and energy among the carriers involved; in QDs, however, quantization of energy levels relaxes the constraint of momentum conservation. Moreover, Coulomb interactions among carriers in QDs are strong, because of their small spatial separation and because of the near absence of electronic and dielectric screening. The result is an Auger recombination time on the order of 10–100 ps, significantly faster than radiative recombination times.

The understanding that has been achieved of carrier dynamics in semiconductor nanocrystals opens up the possibility of engineering the dynamics by controlling the nanocrystal structure. For example, growing a wider-bandgap

DOI: 10.1021/acs.jpcc.7b12629
J. Phys. Chem. C 2018, 122, 10659–10674

shell around a narrower-bandgap core can modify not only trapping rates but also recombination rates. In CdSe/CdS core/shell nanoparticles, the electron wave function extends into the shell, but the hole is confined within the core; thick shells thus lead to decreased electron−hole overlap and thus decreased radiative recombination rates.[27] Auger recombination rates depend on the overlap between the initial and final wave functions of the electron or hole that is excited to higher energy and can thus also be modified by appropriate core/shell structures.[28,29] More dramatic changes in carrier dynamics can be obtained by growing nonspherical nanocrystals, such as rods that confine carriers in two dimensions rather than three.[30] In colloidal nanorods, carrier relaxation occurs through a continuum of states[31] and is thus qualitatively different from the sequential relaxation through discrete states that is observed for QDs. Auger recombination rates have also been observed to be slower in nanorods than in QDs, most likely due to greater spatial separation of the carriers that are involved.[32] Even more complexity is introduced through the growth of branched structures[33,34] or core/shell structures[35,36] that provide a combination of two-dimensional and three-dimensional confinement; for example, measurements imply that carrier-relaxation rates in these mixed-confinement structures are slowed to the point where they are comparable to radiative recombination rates.[37,38]

Despite great progress in controlling nanocrystal structure, the remaining geometry, in which carriers are confined quantum mechanically in only one dimension, was not realized until the past decade. Such nanocrystals can be referred to as "colloidal quantum wells (QWs)," in analogy to the QWs that have been produced in III−V semiconductors since the 1980s using epitaxial deposition techniques such as molecular beam epitaxy and metal−organic chemical vapor deposition.[39] (These colloidal quantum wells should not be confused with the earlier synthesized "quantum dot quantum wells," nanocrystal heterostructures that consist of a low-bandgap inner shell sandwiched between a high-bandgap core and outer shell, but in which carrier confinement is still fully three dimensional.[40]) Colloidal QWs provide a complementary system to epitaxial QWs, with the same basic electronic structure but with several significant differences: (1) colloidal synthesis can produce macroscopic quantities of QWs, each with submicron lateral dimensions, whereas epitaxial QWs are grown one at a time on wafers with lateral dimensions of several inches; (2) colloidal QWs can be synthesized and processed using benchtop solution-based methods, whereas epitaxial QWs are grown using high-cost deposition systems on lattice-matched substrates; (3) colloidal QWs are most commonly made of II−VI semiconductors, whereas epitaxial QWs are most commonly made of III−V semiconductors; and (4) colloidal QWs are free-standing nanoscale structures capped with organic molecules, whereas epitaxial QWs are embedded coherently in a semiconductor matrix. These different characteristics enable different applications and lead to qualitatively different carrier dynamics in the two classes of materials. Carrier dynamics in colloidal QWs are similarly qualitatively different from those in colloidal QDs. This Article reviews the novel carrier dynamics that have been observed in colloidal QWs and the applications that these dynamics enable, particularly the use of colloidal QWs as gain materials for lasers.

2. SEMICONDUCTOR NANOPLATELETS

Colloidal QWs were discovered by modifying the synthesis methods that are used to produce colloidal QDs. The first colloidal QWs to be produced were cadmium chalcogenide nanoribbons with a wurtzite crystal structure.[41,42] CdSe nanoribbons are synthesized through the Lewis acid−base reaction of $CdCl_2$(*n*-octylamine)$_2$ with octylammonium selenocarbonate or cadmium acetate with selenourea;[43] other chalcogenide nanoribbons are produced using corresponding precursors. Shortly afterward, the synthesis of zinc-blende cadmium calcogenide nanoplatelets (NPLs) was demonstrated;[44,45] Figure 2 shows an example of the structures that can be produced. NPLs are produced through the high-temperature reaction of a mixture of Cd precursors with short-chain and long-chain carboxylates (such as cadmium myristate and cadmium acetate) with a chalcogenide precursor (as a complex with trioctyl phosphate or as a powder in a solvent such as octadecene).

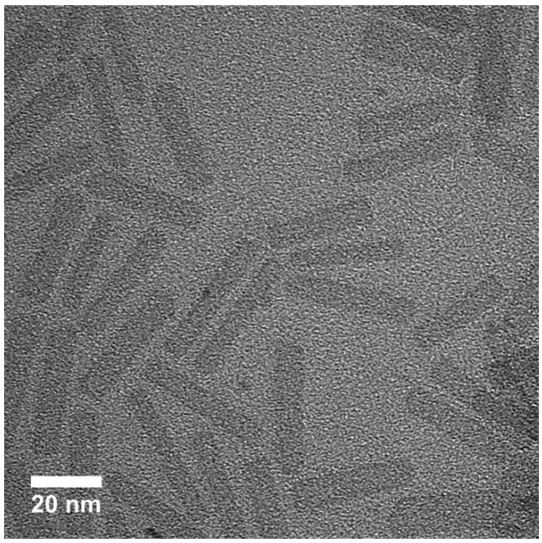

Figure 2. Top-down transmission-electron-microscope (TEM) image of CdSe nanoplatelets (NPLs) with thickness of 4.5 monolayers (ML). Reprinted from ref 72. Copyright 2012 American Chemical Society.

Lateral dimensions of the NPLs are generally on the order of 10−100 nm and are determined by the reaction time.[46] The NPL thicknesses range from 2.5 to 5.5 monolayers (ML), and are determined by the reaction temperatures and the length of the aliphatic chains on the Cd precursors. (In this Article, one ML refers to a single unit cell, or one lattice constant.) Perhaps the most remarkable aspect of the NPL synthesis is that control over the reaction conditions can control the thickness of the resulting NPLs with single-ML precision.[47] That is, not only can the reaction be tuned to increase or decrease the NPL thickness by one monolayer, but all the NPLs in the ensemble have the same thickness to within a single atomic layer. This is reflected in the narrow ensemble PL and absorption line widths, shown in Figure 3, which are nearly identical to the measured line width for a single NPL.[48] Although there is variation in the lateral dimensions of the NPLs, these dimensions are much larger than the Bohr diameter of excitons in the NPLs, so that only the thickness of the NPLs has a significant effect on their transition energies. The lack of inhomogeneous broadening is thus a result of all NPLs having exactly the same thickness. It is also worth noting that the

DOI: 10.1021/acs.jpcc.7b12629
J. Phys. Chem. C 2018, 122, 10659−10674

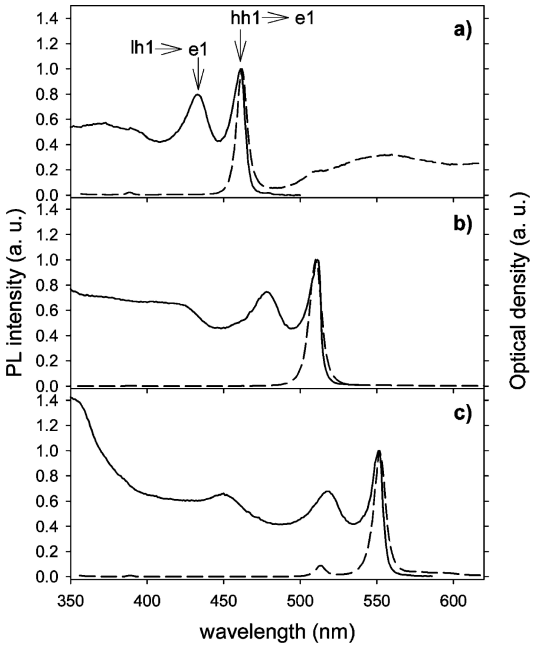

Figure 3. Room-temperature photoluminescence spectra (dashed lines) and absorption spectra (solid lines) for colloidal CdSe nanoplatelets synthesized under different conditions. The nanoplatelets have thicknesses of (a) 3.5, (b) 4.5, and (c) 5.5 monolayers (ML). Reprinted from ref 44. Copyright 2008 American Chemical Society.

narrow absorption and emission lines suggest that there is little variation in thickness across any individual NPL: monolayer thickness fluctuations, as are typical for epitaxial QWs, would lead to varying lateral confinement of excitons at different positions in the NPL and would thus broaden the transitions. The narrow emission lines also indicate that the observed luminescence arises entirely from the NPLs and does not include any measurable contribution from small nanocrystals or other byproducts than may be present in the solution.

The spectra in Figure 3 were acquired at room temperature, illustrating another remarkable property of the NPLs: bound excitons dominate optical absorption and emission from NPLs, even at room temperature.[44,47,49] Two low-energy exciton peaks are clearly resolved in the absorption spectra, one involving a heavy hole and an electron (labeled "hh1 → e1" in Figure 3a), and the other involving a light hole and an electron (labeled "lh1 → e1" in Figure 3a). The exciton binding energy must therefore be large compared to room-temperature thermal energy. The strong exciton binding energy is a result of the confinement of carriers within the colloidal QWs, including both quantum-mechanical confinement (leading to greater electron−hole wave function overlap) and dielectric confinement (i.e., reduced screening of the Coulomb interaction between the electron and the hole).[50] In the limit of perfect two-dimensional confinement, the binding energy would be a factor of 4 larger than in the bulk.[51] For real colloidal QWs, the factor is somewhat smaller because of the finite thickness of the QWs and because the surrounding medium has a finite dielectric constant and partially screens Coulomb interactions within the QWs. The dielectric constants of the organic molecules and solvents that typically surround colloidal QWs are significantly smaller than those of the semiconductor materials that typically surround epitaxial QWs.[39] The binding energies in colloidal QWs are thus significantly higher than in epitaxial QWs and have been calculated to be in the range of 100−400 meV, depending on the QW thickness.[49,52] Few direct measurements of binding energies have been made for colloidal QWs, but measurements of exciton polarizability when a DC electric field is applied to NPLs indicate a binding energy of approximately 170 meV for 5.5-ML-thick CdSe NPLs embedded in a polymer film, in reasonable agreement with calculations.[53]

Quantitative comparison of experimental and calculated exciton binding energies is difficult, because the dielectric constant of the material surrounding NPLs is generally not well known. For NPLs in solution, the packing density and conformation of capping molecules is difficult to characterize; for NPLs deposited as films, the surface configurations are even more complex, and the density and arrangement of the NPLs themselves can have significant effects on the effective dielectric constant of the film. These challenges led to an initial misidentification of NPL thickness based on comparison between calculated and measured transition energies.[47] This misidentification was aided by distortion of the NPL crystal lattice as compared to bulk[54] so that dividing the apparent NPL thickness in transmission-electron-microscope (TEM) images by the bulk lattice constant gave an incorrect number of monolayers. Later studies suggested the need for reinterpretation of NPL thickness,[49] which was confirmed by high-resolution cross-sectional TEM images of NPLs.[55,56] These images also verified the expectation that both faces of the NPLs are terminated with planes of Cd atoms. The cross-sectional thickness of the NPLs thus consists of a half-integer number of unit cells, and this Article refers to thicknesses in this way (e.g., "2.5 ML," "3.5 ML").

Following the examples of colloidal-QD and nanorod heterostructures, the synthesis of NPLs was soon followed by the growth of colloidal-QW heterostructures. The most straightforward heterostructures to synthesize are "core/crown," or in-plane heterostructures, which can be produced by continuing the lateral growth of NPLs with a different anionic precursor.[57,58] The growth of core/shell structures, where the entire NPL is coated by an epitaxial shell of a different semiconductor, was also demonstrated using a different one-pot procedure, but the resulting shells had uneven thicknesses.[55] As in the case of core/shell QDs, the growth of the shell increased PL QYs, but the reproducibility of this synthesis was limited.[59] A more complex but better-controlled shell growth method, named "colloidal atomic layer deposition (c-ALD)," was shown to reproducibly result in high-QY samples with uniform shells (see Figure 4).[60] This method was developed in analogy to gas-phase ALD, in which thin films are deposited with single-ML precision through an alternating series of self-limiting half-reactions.[61] In c-ALD, NPLs or reagants are transferred sequentially between immiscible polar and nonpolar phases, with the growth of a single, complete atomic layer (half a ML) upon each transfer.

Because the shells are grown one atomic layer at a time, the c-ALD process preserves the single-ML monodispersity of the NPL ensembles. Inhomogeneous broadening due to variations in NPL thickness is thus expected to still be absent. This was confirmed by measuring photoluminescence excitation (PLE) spectra for core/shell NPL ensembles at different emission wavelengths.[56,60] For inhomogeneously broadened QDs, monitoring emission at a particular wavelength selects a subensemble of the QDs whose emission overlaps most strongly with the monitored wavelength. PLE spectra for

DOI: 10.1021/acs.jpcc.7b12629
J. Phys. Chem. C 2018, 122, 10659−10674

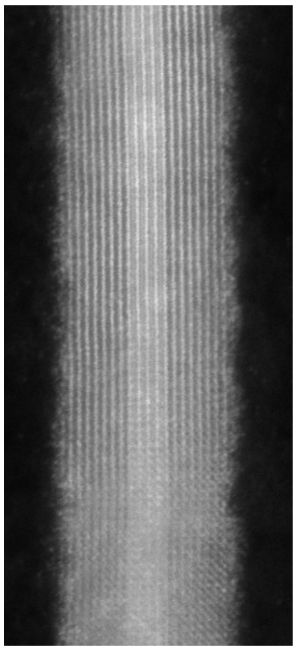

Figure 4. Cross-sectional image of a CdSe/CdS core/shell NPL with core thickness of 4.5 monolayers (ML) and shell thickness of 6 ML. Reprinted from ref 67. Copyright 2017 American Chemical Society.

different emission wavelengths thus correspond to different subensembles of the QDs and are different from one another.[62,63] For NPLs, including core/shell NPLs grown by c-ALD, PLE spectra are independent of emission wavelength, indicating that all NPLs in the ensemble have the same emission spectrum.

The absence of any inhomogeneous broadening that arises from differences in the NPL thicknesses simplifies the job of the optical spectroscopist. For most nanoparticles, ensemble measurements result in complex, weighted averages of the optical properties being measured. For NPLs, spectral variations among nanoparticles have been eliminated, and ensemble measurements can thus be used to determine quantitative structure−property relationships.

3. CARRIER RECOMBINATION

The most common optical-spectroscopy measurement performed on colloidal QWs is PL, in which a short-wavelength light source is used to excite carriers in the QWs well above the bandgap. Light is emitted from the QWs when these carriers bind into excitons, relax to the band edge, and recombine radiatively, with relaxation and radiative recombination competing with carrier trapping and nonradiative recombination. (See Figure 1.) Time-resolved PL measurements thus provide access to the various dynamical processes that carriers experience in the nanoparticles; this Article focuses on the results of such measurements.

Specifically, a measurement of the total PL intensity emitted by an NPL sample as a function of time after excitation by a laser pulse tracks the population of excitons in the luminescent NPLs in the sample. If the sample is weakly excited, so that the average number of excitons produced by the laser pulse in each NPL is much less than one, then a time-resolved PL measurement provides information about single-exciton recombination dynamics—that is, the combination of radiative and nonradiative recombination. Such measurements give average room-temperature exciton recombination times in CdSe NPLs of approximately 200−300 ps. As in CdSe QDs, the ground state is expected to be a dark exciton, and room-temperature emission is expected to come primarily though thermal excitation of the bright-exciton state.[22,23] These expectations were confirmed through temperature-dependent and magnetic-field-dependent time-resolved PL measurements, and average bright-exciton and dark-exciton lifetimes were inferred from the measurements.

It is difficult, however, to ascribe a great deal of physical meaning to measured average lifetimes, because the PL decay curves in all measurements are far from single-exponential decays. Multiple decay times in ensemble measurements could in principle be a result of heterogeneity of NPLs in the ensemble, with different populations of NPLs having different decay dynamics; however, this cannot explain the nearly identical multiexponential decay observed on nanosecond time scales for single NPLs, as illustrated in Figure 5a.[48] Another possible source of complex dynamics is "dynamical," rather than structural, heterogeneity: the recombination rate inside individual NPLs can fluctuate over time, leading to multi-exponential decay in a time-averaged measurement. This is

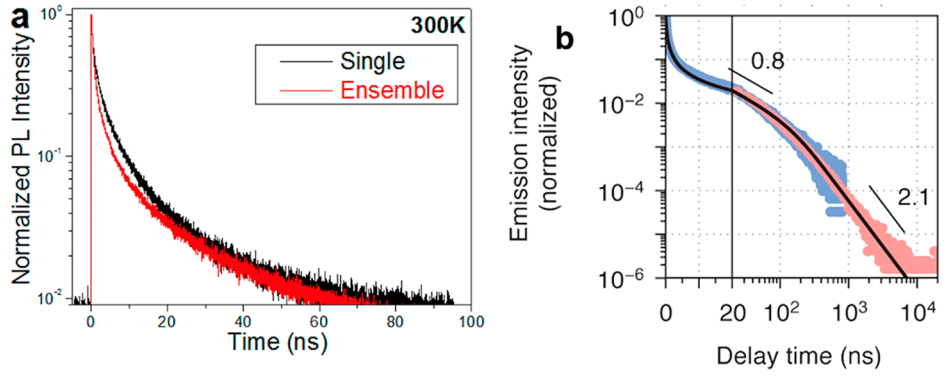

Figure 5. (a) Photoluminescence (PL) intensity from 5.5-monolayer (ML)-thick CdSe nanoplatelets (NPLs) at room temperature, as a function of time after excitation by a laser pulse. Results are shown for an ensemble of NPLs and for a single NPL. Reprinted from ref 48. Copyright 2012 American Chemical Society. (b) PL intensity from an ensemble of 4.5-ML CdSe NPLs as a function of time after excitation. Data are plotted on a semilogarithmic scale for the first 20 ns and on a double-logarithmic scale from 20 ns to 20 μs. Blue and red points are from separate measurements at different time resolutions. Reprinted from ref 71. Copyright 2016 American Chemical Society.

DOI: 10.1021/acs.jpcc.7b12629
J. Phys. Chem. C 2018, 122, 10659−10674

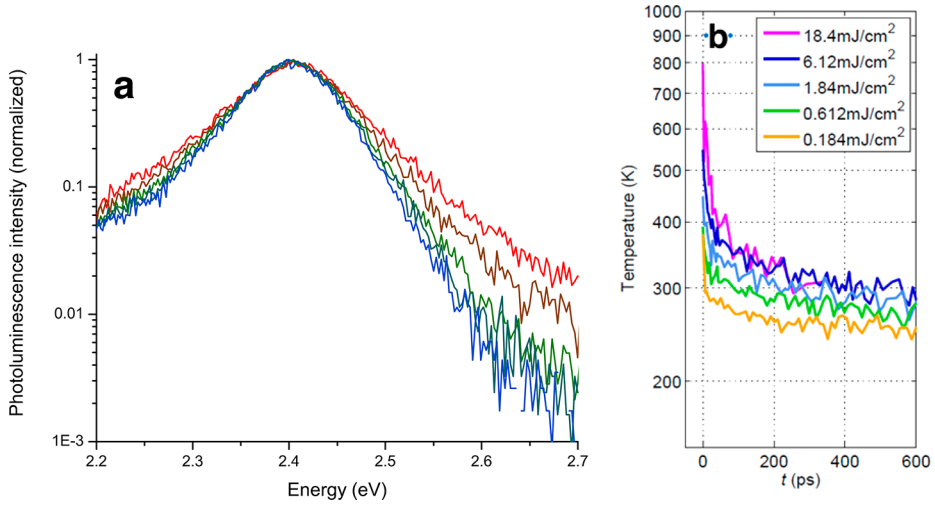

Figure 6. (a) Photoluminescence spectra for 4.5-monolayer (ML)-thick CdSe nanoplatelets (NPLs) at various times following excitation by an ultrafast laser pulse. Spectra are normalized by their maximum value. Lines from top to bottom are for 0, 7, 14, 20, and 27 ps after excitation with a short laser pulse. Reprinted from ref 72. Copyright 2012 American Chemical Society. (b) Carrier temperature in 4.5-ML NPLs as a function of time, *t*, after excitation by ultrafast laser pulses, for different laser-pulse fluences. Reprinted from ref 79. Copyright 2015 American Chemical Society.

commonly observed in colloidal QDs[64] and is connected to PL intermittency, or "blinking."[65] The emission from individual QDs turns "off" and "on" because of jumps in the nonradiative recombination rate, with the "off" state corresponding to fast nonradiative recombination and the "on" state corresponding to slow nonradiative recombination. Blinking has been observed in the emission from single NPLs;[48] if the mechanism is similar to that in QDs, then the measured PL dynamics would represent a weighted average over the lifetimes in the "on" and "off" states. This would result in biexponential decay, with the shorter time constant corresponding approximately to the nonradiative lifetime and the longer time constant corresponding to the radiative lifetime. Analyzing time-resolved PL measurements according to this model yielded a radiative lifetime of 220 ps for CdSe NPLs and 230 ps for CdSe/CdS core/shell NPLs.[66]

Other time-resolved PL measurements, however, have required three[67] or four[68] exponential components to fit the decay curves. The fastest decay component, with a lifetime of approximately 50 ps, can still be attributed to nonradiative recombination, and the decay component with a lifetime of 200−300 ps can still be attributed to radiative recombination. However, slower decay components have also been observed, with lifetimes in the ranges of 1−3 ns, 15−25 ns, and 80−100 ns. Since the PL QY from the NPLs is, in the absence of significant trapping, given by the ratio of the radiative recombination rate to the total recombination rate, QY measurements can give insight into the nature of the measured decay constants; such an analysis is consistent with all of the decay times except the very shortest corresponding to radiative processes.[68] The interpretation of the longer decays as being radiative is further supported by the observation that they are all modified by approximately the same factor when the NPLs are coupled to an optical cavity.[69] Placing an emitter inside an optical cavity enhances its spontaneous emission rate, because spontaneous emission is a result of interaction between the emitter and its local electromagnetic environment.[70] Since this emission enhancement affects only radiative processes, modification of the NPL lifetimes indicates that they correspond to radiative recombination. It is not yet clear, however, what the physical explanation is for the existence of multiple radiative lifetimes in individual NPLs.

Even more complex PL dynamics are observed on longer time scales.[71] As illustrated in Figure 5b, the nanosecond-scale multiexponential decay is followed by a power-law decay that extends to time scales up to 10 μs. The PL spectrum at these long time delays is nearly identical to the spectrum at short time delays, indicating that the same transition is involved in both cases. The slow dynamics were therefore attributed to transfer of one of the charge carriers from the emissive state to a trap state, followed by its transfer back to the emissive state some time later.

4. CARRIER RELAXATION

Information about relaxation of electrons and holes can also be obtained from time-resolved PL measurements if the spectrum, and not only the total intensity, of the emitted light is measured as a function of time after excitation.[72] Figure 6a shows representative results from a sample of CdSe NPLs; a high-energy tail is apparent on the spectra for short time delays. Since the energy of emitted photons corresponds to the energy difference between the recombining electron and hole, the shape of this tail corresponds to the distribution of carrier energies (assuming that the transition matrix elements and the joint density of states are approximately independent of energy over the measured energy range). On a logarithmic scale, the tail is a straight line, corresponding to a Boltzmann distribution of carrier energies

$$I(\hbar\omega) \propto \exp\left(-\frac{\hbar\omega}{k_B T}\right) \quad (1)$$

where ω is the photon frequency, T is the effective carrier temperature, and k_B is Boltzmann's constant. This indicates that the carriers reach internal thermal equilibrium on a time scale fast compared to the few-picosecond time resolution of the measurement. They initially equilibrate at a high effective temperature, and their temperature gradually reduces as they relax toward the band edges. This is qualitatively different from the case of QDs, where carriers cascade downward sequentially through discrete quantum-confined states,[15,73] and demon-

DOI: 10.1021/acs.jpcc.7b12629
J. Phys. Chem. C 2018, 122, 10659−10674

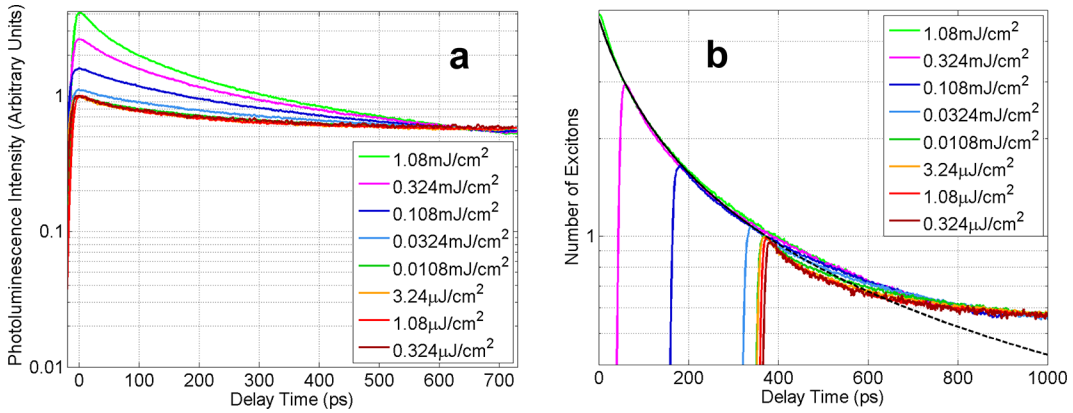

Figure 7. (a) Photoluminescence (PL) intensity as a function of time after pulsed excitation from CdSe/CdS core/shell nanoplatelets (NPLs) with CdSe core thickness of 4.5 monolayers (ML) and CdS shell thickness of 4 ML. Data are shown for different excitation-pulse fluences and are normalized so that they approach the same intensity at long delay times. (b) Average number of excitons per NPL, $N(t)$, as a function of time after excitation. Results are obtained by shifting the luminescence intensities, without normalization, in time so that they fall onto the same curve. Also shown is a fit (black line) to a model of biexcitonic Auger recombination. Reprinted from ref 67. Copyright 2017 American Chemical Society.

strates that a continuous density of states is indeed available for carriers in NPLs. It is also worth noting that emission is observed only for energies near the exciton transition energy, indicating that the electron−hole pairs that are excited by the incident laser pulse bind into excitons on subpicosecond time scales, and the carriers are already bound into excitons as they relax.

The carrier temperature at a given time after excitation can be determined, following eq 1, from the slope of the high-energy tail of the corresponding PL spectrum; representative results are shown in Figure 6b. An initial fast decay is observed but is not well resolved by these measurements. Time-resolved two-photon photoemission measurements on CdSe and CdSe/CdS NPLs have shown electron cooling with time constants below 2 ps,[74] which was explained as being due to rapid emission of LO phonons. Rapid LO-phonon cooling has been observed in bulk semiconductors, including CdSe,[75] and in epitaxial quantum wells.[76] In these materials, the rapid cooling is followed by a slower cooling phase, because LO phonons are generated more quickly than they can decay into acoustic phonons or diffuse away from the excitation region.[77,78] The resulting population of LO phonons returns heat back to the carriers, and the carrier cooling rate is limited by the rate at which the LO-phonon population decays. As shown in Figure 6b, the initial rapid cooling of carriers in CdSe NPLs is followed by a slow relaxation, and it may initially seem that this could be explained by the same "hot-phonon" effect. However, the observed cooling time in the NPLs is on the order of 100 ps, much longer than the approximately 10 ps LO-phonon lifetime.

Instead, the slow relaxation is a consequence of Auger heating,[79] as previously observed in colloidal nanorods.[31] As the carriers cool through the emission of phonons, they are heated through the Auger recombination of other carriers. When an exciton undergoes Auger recombination, the energy it releases is transferred to a carrier in another exciton; this high-energy carrier rapidly exchanges its energy with the other carriers in the NPL, increasing their effective temperature. This Auger reheating competes with cooling through phonons, thereby determining the overall dynamics of carrier relaxation.

5. AUGER RECOMBINATION

The importance of Auger heating illustrates the overall significance of Auger recombination in colloidal QWs. Auger recombination dynamics can be studied more directly by returning to the total time-dependent PL intensity but now making measurements at high excitation powers, so that each incident laser pulse excites multiple excitons into each NPL.[79,80] Representative results are shown in Figure 7a. These decay curves have been normalized to their values at 650 ps to emphasize the subnanosecond decay component that increases in relative magnitude and becomes faster as the energy in the pump pulse increases. This is a sign of a multicarrier process; more specifically, since the carrier-relaxation experiments have shown that excitons are created on the subpicosecond time scale and are highly stable at room temperature, the high-excitation dynamics correspond to multiexciton recombination.

In experiments involving colloidal QDs, multiexciton recombination is most commonly analyzed by including an exponential term for each combination of excitons that can undergo recombination.[5] In NPLs, where the number of excitons can become large, this becomes impractical. Instead, we approximate the exciton number as a continuous variable, $N(t)$, and we consider only biexcitonic Auger recombination, ignoring both single-exciton recombination and processes such as trapping that involve free carriers.[79] We further assume that the rate of biexcitonic Auger recombination is proportional to the square of the exciton number. With these approximations, which should hold for $N(t) > 2$, we can write

$$\frac{dN(t)}{dt} = -AN^2(t) \tag{2}$$

where we call coefficient A the Auger recombination rate. Solving eq 2 gives

$$N(t) = \frac{N(0)}{1 + AN(0)t} \tag{3}$$

Eq 3 indicates that the Auger recombination dynamics at time t depend only on the exciton number, $N(t)$, at that time.[79] In other words, exciting the sample with a high pump fluence leads to a large initial number of excitons per nanoplatelet, $N(0)$; once the exciton population decays from this initial value

DOI: 10.1021/acs.jpcc.7b12629
J. Phys. Chem. C 2018, 122, 10659−10674

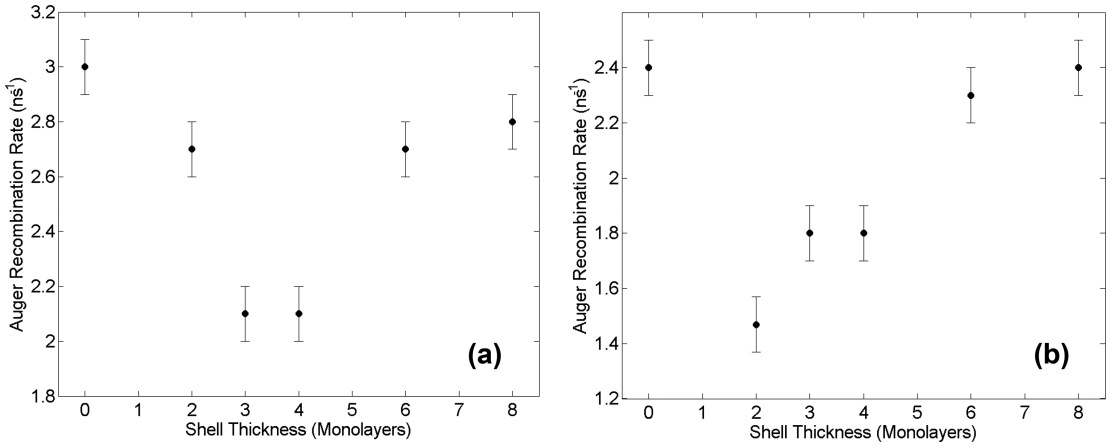

Figure 8. (a) Auger recombination rate as a function of shell thickness for CdSe/CdS core/shell nanoplatelets with core thicknesses of (a) 4.5 monolayers (ML) and (b) 5.5 monolayers (ML). Reprinted from ref 67. Copyright 2017 American Chemical Society.

to a lower value, N_1, the subsequent dynamics are the same as the dynamics obtained when the sample is excited with a lower-fluence pulse that produces N_1 excitons to begin with. Since the measured PL decay intensity is proportional to $N(t)$, it should thus be possible to shift the PL decay curves for different excitation fluences along the time axis and make them all overlap, resulting in a "universal" decay curve that reflects the underlying Auger recombination dynamics. This is demonstrated for a representative data set in Figure 7b. In this figure, biexcitonic Auger recombination dominates the exciton dynamics for time scales less than approximately 300 ps. At longer times, the average exciton number is less than or equal to 1; in this regime, no NPL is likely to be occupied by more than one exciton, and the dynamics are independent of pump fluence.

Figure 7b also shows a fit of the multiexciton dynamics to eq 3. Values of the Auger coefficient A determined from this and equivalent fits are summarized in Figure 8 for CdSe/CdS core/shell NPLs with different core and shell thicknesses.[67] It can be seen that, for both core thicknesses, the Auger coefficient initially decreases as shell thickness increases, reaching a minimum for shell thickness of 3−4 ML, and then increases again with further increases in shell thickness. This nonmonotonic behavior contrasts with the previous observation of a monotonic dependence of Auger rate on thickness of CdSe-only NPLs[81] and also contrasts with previous observations of a monotonic decrease in Auger rate with increasing shell thickness for CdSe/CdS core/shell QDs.[82] However, the QD measurements involved ensembles of nanocrystals that necessarily had a distribution of core and shell thicknesses; since Auger rates are sensitive to small changes in the nanocrystal dimensions, it is possible that an underlying nonmonotonic dependence exists for QDs, but could not be observed because of the averaging effects of this polydispersity.

6. OPTICAL GAIN

The ability to reduce the Auger recombination coefficient in NPLs by growing a shell of appropriate thickness implies that it should be possible to engineer NPL structures in order to minimize threshold power densities for optical gain and lasing. Indeed, reducing Auger rates has been an important strategy for the reduction of thresholds for colloidal QDs.[83,84] An alternative strategy is to engineer the QD structure so that population inversion can be obtained at a lower exciton density; the total Auger recombination rate will thus be lower at threshold, even if the Auger constants in the QDs remain high. This was accomplished by designing QD heterostructures so that optical absorption by an unoccupied QD and emission by a QD that contains a single exciton occur at significantly different energies; a single exciton is thus sufficient to invert a QD.[85,86] Recently, even lower thresholds were obtained by growing QDs with strong anisotropic strain that lifts the degeneracy of the valence band; these QDs enabled CW gain and lasing at room temperature.[87] The QW electronic structure of NPLs presents a similar advantage: because of the large density of states at the band edge, population inversion can be obtained without requiring the high exciton densities that are required in conventional QDs.

Aside from reduced Auger rates at the exciton densities required for inversion, NPLs have two additional advantages over conventional colloidal QDs in terms of reducing gain and lasing thresholds. The first is their large optical absorption cross section, which is simply due to their large physical volumes. This reduces the threshold under optical pumping, as previously observed for colloidal nanorods.[88] More significantly, there is essentially no variation in the emission energies among the NPLs within an ensemble, because they all have the same thickness. For an ensemble of QDs in a laser cavity, only the fraction of nanocrystals whose emission overlaps with the cavity line will contribute to gain; for an ensemble of NPLs, all the nanocrystals will contribute. These advantages are obtained while retaining the fast intraband relaxation, relatively slow interband recombination, and high luminescence QY that are required for a high-quality optical gain material.

The optical gain properties of semiconductor materials are often characterized using measurements of amplified spontaneous emission (ASE).[89] Most commonly, the gain material is deposited as a thin film on a substrate, and the film is excited from normal incidence using a laser beam that is focused into a stripe. Spontaneous emission occurs along the length of the stripe, and some of the emitted light is trapped in the film by total internal reflection and guided along the stripe. This guided emission can then produce stimulated emission, resulting in optical gain. ASE occurs when the gain due to stimulated emission exceeds the losses due to absorption and scattering, and the emitted intensity increases exponentially along the stripe. For a given stripe length, this occurs at a particular threshold pump power density. Experimentally, the threshold

DOI: 10.1021/acs.jpcc.7b12629
J. Phys. Chem. C 2018, 122, 10659−10674

can be identified through the emergence of a narrow-line width stimulated-emission peak on the broader spontaneous-emission background and an increase in the slope in a graph of the output power as a function of the input power.

Both of these ASE properties are illustrated, for representative films of CdSe NPLs and CdSe/CdS core/shell NPLs, in Figure 9.[56] As shown in the inset of Figure 9c, measurements

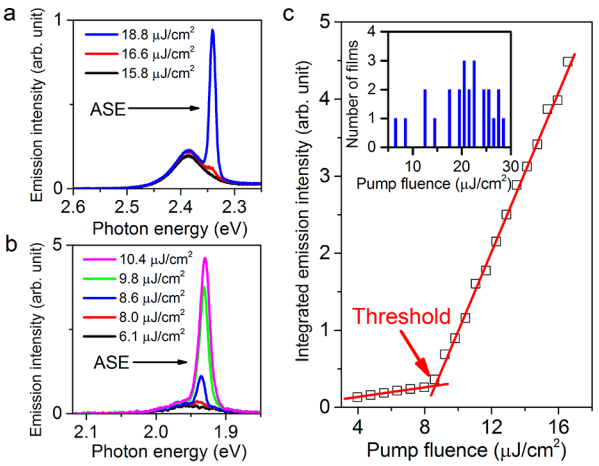

Figure 9. (a,b) Photoluminescence (PL) spectra from films of nanoplatelets (NPLs), for pulsed excitation with different pump fluences. Results are shown for (a) 4.5-monolayer (ML)-thick CdSe NPLs and (b) CdSe/CdS core/shell NPLs with 4.5-ML cores and 3-ML shells. (c) Normalized integrated emission intensity from the film of core/shell NPLs as a function of pump fluence. The dots are experimental data, and the red lines are two linear fits for different regions of pump fluence. The inset shows a histogram of the amplified spontaneous emission (ASE) thresholds for different films of core/shell NPLs with 4.5-ML cores and 3-ML shells. Reprinted from ref 56. Copyright 2014 American Chemical Society.

on several films produced from the same sample of NPLs showed significant variations in threshold. The thresholds were also observed to be sensitive to the film preparation conditions, particularly the concentration of capping molecules in the NPL solution that was used. If the capping-molecule concentration was too high, the films showed significant optical scattering, most likely due to phase segregation of the excess capping molecules. For low capping-molecule concentrations, on the other hand, NPLs are known to form face-to-face stacks;[90] energy transfer among NPLs in the stacks quenches luminescence,[91] and large stacks can contribute to optical scattering. Thresholds are thus minimized for optically transparent but microscopically disordered films. The trade-off for this random ordering is a lower packing density for the NPLs in the film, and thus a lower gain coefficient. Despite this trade-off, the optimized films showed low ASE thresholds, with the lowest observed threshold of 6 μJ/cm^2 being lower than any previous reports using colloidal nanocrystals,[83,86] and equivalent to the lowest reported threshold at that point using any solution-processed material.[92,93] Similar ASE thresholds were obtained in an independent report,[94] and ASE from NPLs has also been observed under two-photon pumping and for CdSe/CdTe core/crown NPLs.[95]

For a given pump power, there is also a threshold stripe length for ASE. For stripe lengths, l, greater than this threshold, the output intensity increases as e^{Gl}, where G is the modal gain coefficient. Of course, the output power cannot increase indefinitely and eventually saturates with increasing stripe length or pump power. For pulsed excitation of the gain material, this saturation corresponds to the point where stimulated emission fully depletes the gain medium. Measurements of ASE as a function of stripe length thus provide a straightforward means of determining modal gain and saturation threshold; both of these characteristics were observed to be higher for NPLs than previously reported best values for colloidal QDs.[14,83,96] The lowest ASE thresholds and highest modal gains were observed for CdSe/CdS core/shell NPLs with 4.5-ML cores and 3-ML shells. This shell thickness also gives the lowest Auger coefficient (see Figure 8a), validating the importance of minimizing Auger rates in optimizing NPLs as gain materials.

7. LASING

Integration of NPLs into laser cavities followed quickly on the initial demonstration of low ASE thresholds. Using CdSe and CdSe/CdS core/shell NPLs with different core and shell thicknesses, ASE in thin films and lasing in Fabry–Pérot cavities were demonstrated across the entire visible spectrum,[97−99] using one-, two-, and three-photon excitation.[100] Moreover, lasing was reported at room temperature under continuous-wave excitation;[101] this important practical milestone had not previously been realized using solution-processed materials.

These successes raised the prospect of producing NPL lasers with very low thresholds. Minimizing laser threshold requires optimizing not only the NPLs as a gain material but also the optical cavity into which they emit. Reducing the mode volume of the cavity reduces laser threshold by reducing the amount of active material that must be inverted and by increasing the rate at which the active material emits photons into the cavity mode:[70] this increases the fraction, β, of spontaneously emitted light that is coupled into the mode, thereby decreasing the number of photons that must be emitted before stimulated emission overcomes spontaneous emission.

The lowest mode volumes are obtained using plasmonic metal nanoparticles as optical resonators.[102] However, plasmon resonances unavoidably suffer from strong damping[103] so that the resonators have low photon storage times or low optical quality factors, Q. The optimal trade-off between small mode volume and high Q is obtained using photonic-crystal (PC) cavities.[104] A PC is a structure in which the refractive index is modulated periodically on a length scale comparable to the wavelength of light.[105] Interference among multiple reflections in the periodic structure prevents light propagation within a certain frequency range, known as a stop band or photonic band gap. Around a localized defect in the PC lattice, a localized photonic state is formed within the stop band. The localized defect is a type of optical cavity, with the surrounding PC acting as a mirror.

To produce a low-threshold NPL laser, we used a PC cavity fabricated in a suspended nanobeam of silicon nitride.[106] Silicon nitride is chosen as the cavity material because it has a high refractive index, it is transparent at NPL emission wavelengths, and it can be processed into high-quality microstructures using standard semiconductor fabrication tools. The nanobeam geometry is chosen because of the ease of integration of NPLs. The beam acts as a single-mode optical waveguide for light emitted by the NPLs. A one-dimensional PC is formed by milling a line of air holes in the nanobeam, and the cavity is formed by reducing the spacing and radius of holes

DOI: 10.1021/acs.jpcc.7b12629
J. Phys. Chem. C 2018, 122, 10659−10674

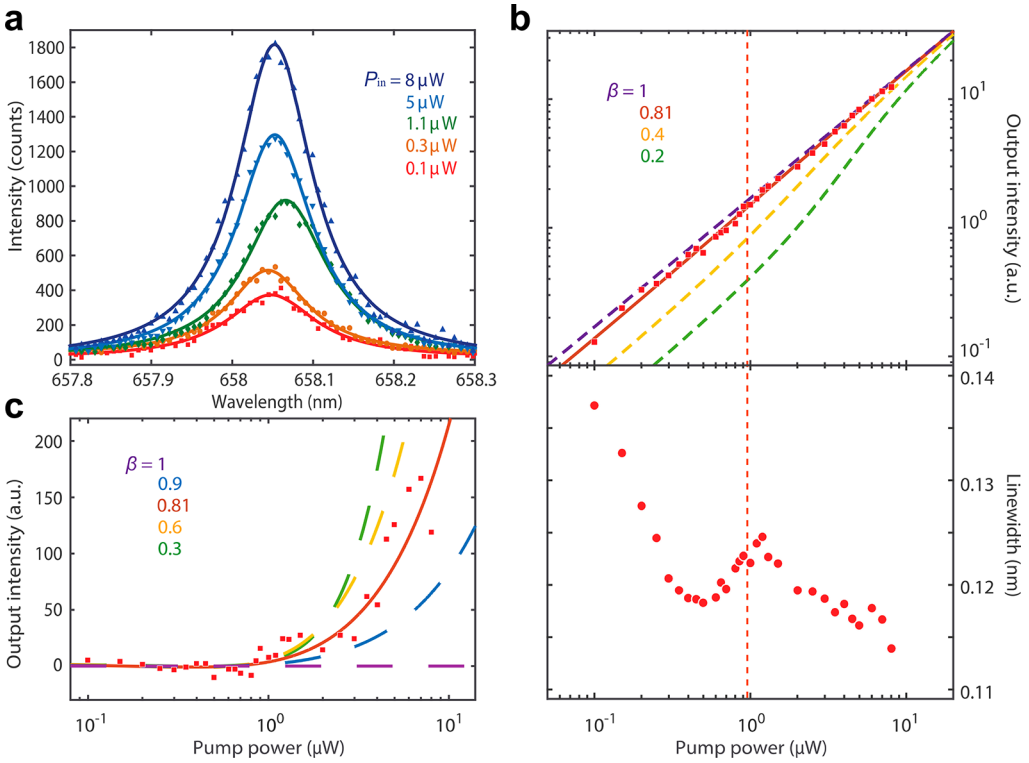

Figure 10. (a) Photoluminescence (PL) spectra from CdSe/CdS core/shell nanoplatelets (NPLs) with 4.5-monolayer (ML)-thick cores and 4-ML-thick shells, deposited on top of a silicon-nitride photonic-crystal nanobeam cavity, for continuous-wave excitation with different pump powers. Symbols indicate the measured data, and the lines are Lorentzian fits. (b) Top: integrated output intensity as a function of pump power. Red squares are measured data, and the solid curve is a fit to the laser rate equation, corresponding to a spontaneous emission coupling efficiency β = 0.81. Dashed curves are calculation results for different values of β. Bottom: emission line width as a function of pump power. The vertical dashed line indicates the laser threshold. (c) Output intensity after subtracting a linear fit to the data points below threshold. Reprinted from ref 69. Copyright 2017 Springer Nature.

in the center of the beam. NPLs are then simply drop-cast on the top surface of the nanobeam; those that are deposited in the center of the cavity are located at the maximum electric field of the cavity mode, and thus couple optimally to the cavity.

Lasing was demonstrated at room temperature by exciting the completed device from the normal direction by using a continuous-wave laser.[69] As shown in Figure 10a, the emission spectrum for NPLs coupled to the cavity is very narrow, even below threshold, because emission into the cavity mode is enhanced above all other emission.[70] The result is a high spontaneous emission coupling factor, β, and thus a "soft" threshold in the plot of output power as a function of input power,[107] as shown in Figure 10b. Lasers with large cavity mode volumes and low β show a dramatic change at threshold in the slope of the input−output curve on a linear scale (similar to the ASE threshold shown in Figure 9c), corresponding to a pronounced "S" shape on a log−log plot, with an inflection point where round-trip gain overcomes loss in the cavity. For microscopic lasers, the inflection becomes less pronounced and eventually disappears as β –> 1, as illustrated by the theoretical curves in Figure 10b. The inflection is nonetheless still present, as can be seen by subtracting a straight line from the data (see Figure 10c).

The conventional definition of laser threshold is the point at which gain overcomes loss and is commonly found by extrapolating a linear fit to the above-threshold input−output curve. However, for lasers with high β, a more appropriate definition of the threshold is the point at which the rate of stimulated emission equals the rate of spontaneous emission, which corresponds to the point where the average photon number in the cavity is unity.[108] This threshold can most accurately be found by fitting the input−output curve to the results of a rate equation,[107] as illustrated in Figure 10b. The threshold is also apparent in the characteristic line width behavior in Figure 10b. Below threshold, the output line width decreases with increasing pump power due to absorption saturation and reduced spontaneous-emission noise. Just below threshold, the line width increases due to gain-index coupling, indicating a dynamic phase transition to lasing.[109] Above threshold, the line width shows characteristic Shawlow−Townes narrowing, due to continued suppression of spontaneous emission noise. This narrowing does not continue indefinitely; rather, the line width appears to approach a minimum value, likely due to heating of the device.

The threshold of this device corresponds to 0.97 μW of incident pump power, lower than previous reports for lasers of any kind operating at room temperature.[110,111] We estimate that 210 nW of this incident power is absorbed by the NPLs at threshold; this threshold in absorbed power is equivalent to the best previous reports for a room-temperature laser.[110] In contrast to many other lasers based on colloidal nanocrystals, the PC-cavity NPL laser is stable under CW operation at room temperature for several hours in a nitrogen environment, with a decrease of only 5% in the measured output power over 2 h of uninterrupted operation.

DOI: 10.1021/acs.jpcc.7b12629
J. Phys. Chem. C 2018, 122, 10659−10674

8. CONCLUSIONS

Semiconductor nanoplatelets confine carriers strongly in only one spatial dimension, thereby acting as colloidal quantum wells. Ensembles of NPLs can be synthesized with thicknesses that are identical to within a single ML, and Auger recombination rates can be minimized by growing core/shell NPLs. The NPLs can thus serve as optical gain materials with low gain thresholds and high gain coefficients. Incorporating the NPLs into a photonic-crystal cavity with small mode volume results in a laser that operates stably under continuous-wave excitation at room temperature, with a threshold lower than that of any previously demonstrated room-temperature laser. The measured threshold is limited almost entirely by the quality factor of the cavity and could be reduced further by improving the fabrication process to provide higher cavity Q.[112]

As well as providing a low threshold, the small mode volume of the PC-cavity NPL laser should enable the laser to have a high modulation bandwidth. The SiN material used for the cavity is compatible with standard photonic processing tools, and the solution processability of the NPLs means that they can readily be incorporated into any materials platform. The lasers thus have the characteristics that are needed to serve as light sources for low-power on-chip optical communication.[113] Realizing this or other practical applications of the lasers will require improvements in the fabrication process to provide higher yields of successful devices, treatment of the NPL surfaces, or encapsulation of the devices to provide long-term stability in ambient operating conditions and to find a route toward electrical injection rather than optical pumping.

PC cavities are not the only ones that can be used for NPL lasers: the NPLs have the potential to provide low-threshold lasing at nearly arbitrary wavelengths, in nearly arbitrary cavity configurations. The broad tunability of the NPL emission enables laser operation in wavelength ranges that are currently difficult to access using semiconductor and solid-state lasers. The solution processability of the NPLs means that the lasers could be integrated onto flexible substrates, into CMOS-compatible substrates and processes, into lab-on-chip diagnostic systems, and into chemical sensing systems. Many of these configurations would likely employ films of NPLs similar to those used for the ASE measurements described above. These films can likely be further improved, using ligand-exchange strategies that have been successful for colloidal QDs,[86,114] so that scattering losses are lower and packing densities of NPLs (and thus gain coefficients) are higher.

Minimization of gain and laser thresholds was achieved, in part, by controlling the core/shell structure of NPLs to minimize Auger rates. Minimization of Auger rates can benefit other potential applications of NPLs, as well. For example, Auger recombination is understood to be at least partially responsible for limiting the efficiency of nanocrystal-based LEDs at high currents.[115,116] Auger recombination can also compete with energy or charge transfer from NPLs to other light emitters. It has already been shown that energy transfer between NPLs can be much faster than energy transfer between QDs and can be efficient, because it is faster than Auger recombination.[117] Further reducing Auger rates could potentially allow the efficiency of energy or charge transfer from NPLs to approach 100%. If NPLs, with their large absorption cross sections, can efficiently transfer charge to high-QY emitters with small absorption cross sections, the result will be a photoluminescent material with minimal reabsorption of emitted light. Such a material could provide an alternative route toward low-threshold optically pumped lasers,[118] and could be used to produce luminescent solar concentrators with high concentration factors and high efficiencies.[119,120]

The first step toward minimizing Auger recombination in NPLs has been provided by the observation that the Auger coefficient in core/shell NPLs has a minimum as a function of shell thickness. This minimum may also exist for colloidal QDs but has been obscured by polydispersity in the QD ensembles that were studied experimentally. Indeed, calculations have predicted oscillations in the Auger recombination rate for core/shell QDs with increasing shell thickness.[121,122] A quantitative understanding of Auger rates in NPLs will require adapting these calculations to the two-dimensional geometry of colloidal QWs, including the challenging task of taking into account the strong electron−hole correlations that are present in these materials. With such an understanding, it may be possible to engineer NPL heterostructures with even smaller Auger coefficients. For example, graded interfaces between the core and the shell have been shown to reduce Auger rates in core/shell QDs,[82,123−125] and a similar approach may be effective for NPLs. Growing a shell with type-II band alignment has also been shown to have a strong effect on Auger recombination.[28,126] So far, type-II NPL heterostructures have been demonstrated only in the core/crown configuration,[127] where the interfacial area between the two materials is small; gain thresholds using these NPLs have been comparable to those achieved using CdSe/CdS core/shell NPLs.[128] It should be possible to extend the c-ALD technique to produce type-II core/shell NPLs, potentially leading to further reductions in gain threshold. Moreover, these type-II colloidal QWs should support spatially indirect excitons with long lifetimes, without requiring the low temperatures that have been required to observe spatially indirect excitons in epitaxial quantum wells.[129,130] Long exciton lifetimes, together with the strong carrier−carrier interactions that are the result of weak screening in colloidal QWs, may provide an opportunity to observe new phenomena based on the interactions of multiple excitons.

Long exciton lifetimes could also be realized by synthesizing NPLs out of materials that have slow intrinsic recombination rates. NPLs of materials other than the cadmium chalcogenides that are the focus of this Article could also provide emission in spectral ranges outside of the visible, eliminate the use of hazardous materials in future applications, and provide access to a broad range of novel physical phenomena. Already, cation exchange has been used to convert CdS NPLs into ZnS and PbS NPLs and CdSe/CdS core/shell NPLs into ZnSe/ZnS and PbSe/PbS core/shell NPLs.[131] It has been proposed that the growth of colloidal NPLs is driven by an intrinsic growth instability,[132] suggesting that NPLs can be produced out of a wide variety of materials if appropriate precursors can be found. Indeed, the versatility of the synthesis method has already been demonstrated through the growth of NPLs of Gd_2O_3,[133] LaF_3,[134] In_2S_3,[135] transition-metal oxides and rare-earth oxides,[136] GeS and GeSe,[137] ZrS_2,[138] transition-metal chalcogenides,[139,140] organihalide perovskites,[141] cesium lead halide perovskites,[142,143] and FeS_2.[132] Access to a nearly unlimited library of materials means that colloidal QWs have the potential to rival van der Waals materials[144] as a platform for exploring the novel phenomena and applications that arise in two-dimensional materials.

DOI: 10.1021/acs.jpcc.7b12629
J. Phys. Chem. C 2018, 122, 10659−10674

AUTHOR INFORMATION

Corresponding Author

*E-mail: mpelton@umbc.edu.

ORCID

Matthew Pelton: 0000-0002-6370-8765

Notes

The author declares no competing financial interest.

Biography

Matthew Pelton received a B.A.Sc. in Engineering Physics from the University of Toronto in 1996 and a Ph.D. in Applied Physics from Stanford University in 2002. Following postdoctoral positions at the Royal Institute of Technology in Sweden and at the University of Chicago, he joined the Center for Nanoscale Materials at Argonne National Laboratory, where he was a scientific staff member from 2006 until 2013. In 2013, he joined the Department of Physics at the University of Maryland, Baltimore County. His research focuses on understanding the dynamics of photoinduced processes at the nanoscale and how they depend on the size, shape, composition, and arrangement of nanostructures, using ultrafast laser spectroscopy and single-particle optical microscopy.

ACKNOWLEDGMENTS

This review is based on work done in collaboration with many people, including Jordan Andrews, Erfan Baghani, Arnaud Demortière, Dmitriy Dolzhnikov, Igor Fedin, Sandrine Ithurria, Haixu Leng, Stephen O'Leary, Richard Schaller, Chungxing She, Dmitri Talapin, Edo Waks, and Zhili Yang. I thank Tim Ford for the cover illustration and TOC image and Alexander Efros and Dmitri Talapin for comments on the manuscript. The work on which this review is based was supported by the National Science Foundation (DMR-0213745, DMR-1420703, DMR-1629601, CHE-1611331), the Air Force Office of Scientific Research (FA9550-14-1-0367), the Office of Naval Research (N000141410612), the Defense Advanced Research Projects Agency, the David and Lucile Packard Foundation, the Keck Foundation, the Samsung Global Research Outreach Program, and the Natural Sciences and Engineering Research Council of Canada, and was performed, in part, at the Center for Nanoscale Materials, a U.S. Department of Energy, Office of Science, Office of Basic Energy Sciences User Facility under contract No. DE-AC02-06CH11357.

REFERENCES

(1) Ekimov, A. I.; Onushchenko, A. A. Quantum Size Effects in Three-Dimensional Microscopic Semiconductor Crystals. *JETP Lett.* **1981**, *34*, 345−349.

(2) Rossetti, A.; Nakahara, S.; Brus, L. E. Quantum Size Effects in the Redox Potentials, Resonance Raman Spectra, and Electronic Spectra of CdS Crystallites in Aqueous Solution. *J. Chem. Phys.* **1983**, *79*, 1086−1088.

(3) Kovalenko, M. V.; Manna, L.; Cabot, A.; Hens, Z.; Talapin, D. V.; Kagan, C. R.; Klimov, V. I.; Rogach, A. L.; Reiss, P.; Milliron, D. J.; et al. Prospects of Nanoscience with Nanocrystals. *ACS Nano* **2015**, *9*, 1012−1057.

(4) Kagan, C. R.; Lifshitz, E.; Sargent, E. H.; Talapin, D. V. Building Devices from Colloidal Quantum Dots. *Science* **2016**, *353*, aac5523.

(5) Pietryga, J. M.; Park, Y.-S.; Lim, J.; Fidler, A. F.; Bae, W. K.; Brovelli, S.; Klimov, V. I. Spectroscopic and Device Aspects of Nanocrystal Quantum Dots. *Chem. Rev.* **2016**, *116*, 10513−10622.

(6) Murray, C. B.; Norris, D. J.; Bawendi, M. G. Synthesis and Characterization of Nearly Monodisperse CdE (E = S, Se, Te) Semiconductor Nanocrystallites. *J. Am. Chem. Soc.* **1993**, *115*, 8706−8715.

(7) Hines, M. A.; Guyot-Sionnest, P. Synthesis and Characterization of Strongly Luminescing ZnS-Capped CdSe Nanocrystals. *J. Phys. Chem.* **1996**, *100*, 468−471.

(8) Resch-Genger, U.; Grabolle, M.; Cavaliere-Jaricot, S.; Nitschke, R.; Nann, T. Quantum Dots Versus Organic Dyes as Fluorescent Labels. *Nat. Methods* **2008**, *5*, 763−775.

(9) Bourzac, K. Quantum Dots Go on Display. *Nature* **2013**, *493*, 283.

(10) Shirasaki, Y.; Supran, G. J.; Bawendi, M. G.; Bulović, V. Emergence of Colloidal Quantum-Dot Light-Emitting Technologies. *Nat. Photonics* **2013**, *7*, 13−23.

(11) Dai, X.; Zhang, Z.; Jin, Y.; Niu, Y.; Cao, H.; Liang, X.; Chen, L.; Wang, J.; Peng, X. Solution-Processed, High-Performance Light-Emitting Diodes Based on Quantum Dots. *Nature* **2014**, *515*, 96−99.

(12) Klimov, V. I.; Mikhailovsky, A. A.; Xu, S.; Malko, A.; Hollingsworth, J. A.; Leatherdale, C. A.; Eisler, H.-J.; Bawendi, M. G. Optical Gain and Stimulated Emission in Nanocrystal Quantum Dots. *Science* **2000**, *290*, 314−317.

(13) Eisler, H.-J.; Sundar, V. C.; Bawendi, M. G.; Walsh, M.; Smith, H. I.; Klimov, V. Color-Selective Semiconductor Nanocrystal Laser. *Appl. Phys. Lett.* **2002**, *80*, 4614−4616.

(14) Malko, A. V.; Mikhailovsky, A. A.; Petruska, M. A.; Hollingsworth, J. A.; Htoon, H.; Bawendi, M. G.; Klimov, V. I. From Amplified Spontaneous Emission to Microring Lasing Using Nanocrystal Quantum Dot Solids. *Appl. Phys. Lett.* **2002**, *81*, 1303−1305.

(15) Klimov, V. I.; McBranch, D. W. Femtosecond 1*P*-to-1*S* Electron Relaxation in Strongly Confined Semiconductor Nanocrystals. *Phys. Rev. Lett.* **1998**, *80*, 4028−4031.

(16) Efros, A. E.; Kharchenko, V. A.; Rosen, M. Breaking the Phonon Bottleneck in Nanometer Quantum Dots: Role of Auger-Like Processes. *Solid State Commun.* **1995**, *93*, 281−284.

(17) Hendry, E.; Koeberg, M.; Wang, F.; Zhang, H.; de Mello Donegá, C.; Vanmaekelbergh, D.; Bonn, M. Direct Observation of Electron-to-Hole Energy Transfer in CdSe Quantum Dots. *Phys. Rev. Lett.* **2006**, *96*, 057408.

(18) Schroeter, D. F.; Griffiths, D. J.; Sercel, P. C. Defect-Assisted Relaxation in Quantum Dots at Low Temperature. *Phys. Rev. B: Condens. Matter Mater. Phys.* **1996**, *54*, 1486.

(19) Guyot-Sionnest, P.; Wehrenberg, B.; Yu, D. Intraband Relaxation in CdSe Nanocrystals and the Strong Influence of the Surface Ligands. *J. Chem. Phys.* **2005**, *123*, 074709.

(20) Pandey, A.; Guyot-Sionnest, P. Slow Electron Cooling in Colloidal Quantum Dots. *Science* **2008**, *322*, 929−932.

(21) Guyot-Sionnest, P.; Shim, M.; Matranga, C.; Hines, M. Intraband Relaxation in CdSe Quantum Dots. *Phys. Rev. B: Condens. Matter Mater. Phys.* **1999**, *60*, R2181.

(22) Nirmal, M.; Norris, D. J.; Kuno, M.; Bawendi, M. G.; Efros, Al. L.; Rosen, M. Observation of the "Dark Exciton" in CdSe Quantum Dots. *Phys. Rev. Lett.* **1995**, *75*, 3728−3731.

(23) Crooker, S. A.; Barrick, T.; Hollingsworth, J. A.; Klimov, V. I. Multiple Temperature Regimes of Radiative Decay in CdSe Nano-

DOI: 10.1021/acs.jpcc.7b12629
J. Phys. Chem. C 2018, 122, 10659−10674

crystal Quantum Dots: Intrinsic Limits to the Dark-Exciton Lifetime. *Appl. Phys. Lett.* **2003**, *82*, 2793−2795.
(24) Peng, X.; Schlamp, M. C.; Kadavanich, A. V.; Alivisatos, A. P. Epitaxial Growth of Highly Luminescent CdSe/CdS Core/Shell Nanocrystals with Photostability and Electronic Accessibility. *J. Am. Chem. Soc.* **1997**, *119*, 7019−7029.
(25) Chen, O.; Zhao, J.; Chauhan, V. P.; Cui, J.; Wong, C.; Harris, D. K.; Wei, H.; Han, H.-S.; Fukumura, D.; Jain, R. K.; et al. Compact High-Quality CdSe-CdS Core-Shell Nanocrystals with Narrow Emission Linewidths and Suppressed Blinking. *Nat. Mater.* **2013**, *12*, 445−451.
(26) Klimov, V. I.; Mikhailovsky, A. A.; McBranch, D. W.; Leatherdale, C. A.; Bawendi, M. G. Quantization of Multiparticle Auger Rates in Semiconductor Quantum Dots. *Science* **2000**, *287*, 1011−1013.
(27) Chen, Y.; Vela, J.; Htoon, H.; Casson, J. L.; Werder, D. J.; Bussian, D. A.; Klimov, V. I.; Hollingsworth, J. A. "Giant" Multishell CdSe Nanocrystal Quantum Dots with Suppressed Blinking. *J. Am. Chem. Soc.* **2008**, *130*, 5026−5027.
(28) Oron, D.; Kazes, M.; Banin, U. Multiexcitons in Type-II Colloidal Semiconductor Quantum Dots. *Phys. Rev. B: Condens. Matter Mater. Phys.* **2007**, *75*, 035330.
(29) Bae, W. K.; Padilha, L. A.; Park, Y.-S.; McDaniel, H.; Robel, I.; Pietryga, J. M.; Klimov, V. I. Controlled Alloying of the Core-Shell Interface in CdSe/CdS Quantum Dots for Suppression of Auger Recombination. *ACS Nano* **2013**, *7*, 3411−3419.
(30) Peng, X.; Manna, L.; Yang, W.; Wickham, J.; Scher, E.; Kadavanich, A.; Alivisatos, A. P. Shape Control of CdSe Nanocrystals. *Nature* **2000**, *404*, 59−61.
(31) Achermann, M.; Bartko, A. P.; Hollingsworth, J. A.; Klimov, V. I. The Effect of Auger Heating on Intraband Carrier Relaxation in Semiconductor Quantum Rods. *Nat. Phys.* **2006**, *2*, 557−561.
(32) Htoon, H.; Hollingsworth, J. A.; Dickerson, R.; Klimov, V. I. Effect of Zero- to One-Dimensional Transformation on Multiparticle Auger Recombination in Semiconductor Quantum Rods. *Phys. Rev. Lett.* **2003**, *91*, 227401.
(33) Manna, L.; Scher, E. C.; Alivisatos, A. P. Synthesis of Soluble and Processable Rod-, Arrow-, Teardrop-, and Tetrapod-Shaped CdSe Nanocrystals. *J. Am. Chem. Soc.* **2000**, *122*, 12700−12706.
(34) Milliron, D. J.; Hughes, S. M.; Cui, Y.; Manna, L.; Li, J.; Wang, L.-W.; Alivisatos, A. P. Colloidal Nanocrystal Heterostructures with Linear and Branched Topology. *Nature* **2004**, *430*, 190−195.
(35) Talapin, D. V.; Koeppe, R.; Götzinger, S.; Kornowski, A.; Lupton, J. M.; Rogach, A. L.; Benson, O.; Feldmann, J.; Weller, H. Highly Emissive Colloidal CdSe/CdS Heterostructures of Mixed Dimensionality. *Nano Lett.* **2003**, *3*, 1677−1681.
(36) Talapin, D. V.; Nelson, J. H.; Shevchenko, E. V.; Aloni, S.; Sadtler, B.; Alivisatos, A. P. Seeded Growth of Highly Luminescent CdSe/CdS Nanoheterostructures with Rod and Tetrapod Morphologies. *Nano Lett.* **2007**, *7*, 2951−2959.
(37) Choi, C. L.; Li, H.; Olson, A. C. K.; Jain, P. K.; Sivasankar, S.; Alivisatos, A. P. Spatially Indirect Emission in a Luminescent Nanocrystal Molecule. *Nano Lett.* **2011**, *11*, 2358−2362.
(38) She, C.; Bryant, G. W.; Demortière, A.; Shevchenko, E. V.; Pelton, M. Controlling the Spatial Location of Photoexcited Electrons in Semiconductor CdSe/CdS Core/Shell Nanorods. *Phys. Rev. B: Condens. Matter Mater. Phys.* **2013**, *87*, 155427.
(39) Weisbuch, C.; Vinter, B. *Quantum Semiconductor Structures: Fundamentals and Applications*, 1st ed.; Academic Press: San Diego, CA, 1991.
(40) Eychmüller, A.; Mews, A.; Weller, H. A Quantum Dot Quantum Well: CdS/HgS/CdS. *Chem. Phys. Lett.* **1993**, *208*, 59−62.
(41) Joo, J.; Son, J. S.; Kwon, S. G.; Yu, J. H.; Hyeon, T. Low-Temperature Solution-Phase Synthesis of Quantum Well Structured CdSe Nanoribbons. *J. Am. Chem. Soc.* **2006**, *128*, 5632−5633.
(42) Yang, J.; Son, J. S.; Yu, J. H.; Joo, H.; Hyeon, T. Advances in the Colloidal Synthesis of Two-Dimensional Semiconductor Nanoribbons. *Chem. Mater.* **2013**, *25*, 1190−1198.
(43) Liu, Y.-H.; Wayman, V. L.; Gibbons, P. C.; Loomis, R. A.; Buhro, W. E. Origin of High Photoluminescence Efficiencies in CdSe Quantum Belts. *Nano Lett.* **2010**, *10*, 352−357.
(44) Ithurria, S.; Dubertret, B. Quasi 2D Colloidal CdSe Platelets with Thicknesses Controlled at the Atomic Level. *J. Am. Chem. Soc.* **2008**, *130*, 16504−16505.
(45) Bouet, C.; Tessier, M. D.; Ithurria, S.; Mahler, B.; Nadal, B.; Dubertret, B. Flat Colloidal Semiconductor Nanoplatelets. *Chem. Mater.* **2013**, *25*, 1262−1271.
(46) Ithurria, S.; Bousquet, G.; Dubertret, B. Continuous Transition from 3D to 1D Confinement Observed During the Formation of CdSe Nanoplatelets. *J. Am. Chem. Soc.* **2011**, *133*, 3070−3077.
(47) Ithurria, S.; Tessier, M. D.; Mahler, B.; Lobo, R. P. S. M.; Dubertret, B.; Efros, Al. L. Colloidal Nanoplatelets with Two-Dimensional Electronic Structure. *Nat. Mater.* **2011**, *10*, 936−941.
(48) Tessier, M. D.; Javaux, C.; Maksimovic, I.; Loriette, V.; Dubertret, B. Spectroscopy of Single CdSe Nanoplatelets. *ACS Nano* **2012**, *6*, 6751−6758.
(49) Achtstein, A. W.; Schliwa, A.; Prudnikau, A.; Hardzei, M.; Artemyev, M. V.; Thomsen, C.; Woggon, U. Electronic Structure and Exciton-Phonon Interaction in Two-Dimensional Colloidal CdSe Nanosheets. *Nano Lett.* **2012**, *12*, 3151−3157.
(50) Hanamura, E.; Nagaosa, N.; Kumagai, M.; Takagahara, T. Quantum Wells with Enhanced Exciton Effects and Optical Non-linearity. *Mater. Sci. Eng., B* **1988**, *1*, 255−258.
(51) Ralph, H. I. The Electronic Absorption Edge in Layer Type Crystals. *Solid State Commun.* **1965**, *3*, 303−306.
(52) Benchamekh, R.; Gippius, N. A.; Even, J.; Nestoklon, M. O.; Jancu, J.-M.; Ithurria, S.; Dubertret, B.; Efros, Al. L.; Voisin, P. Tight-Binding Calculations of Image-Charge Effects in Colloidal Nanoscale Platelets of CdSe. *Phys. Rev. B: Condens. Matter Mater. Phys.* **2014**, *89*, 035307.
(53) Scott, R.; Achtstein, A. W.; Prudnikau, A. V.; Antanovich, A.; Siebbeles, L. D. A.; Artemyev, M.; Woggon, U. Time-Resolved Stark Spectroscopy in CdSe Nanoplatelets: Exciton Binding Energy, Polarizability, and Field-Dependent Radiative Rates. *Nano Lett.* **2016**, *16*, 6576−6853.
(54) Chen, D.; Gao, Y.; Chen, Y.; Ren, Y.; Peng, X. Structure Identification of Two-Dimensional Colloidal Semiconductor Nanocrystals with Atomic Flat Basal Planes. *Nano Lett.* **2015**, *15*, 4477−4482.
(55) Mahler, B.; Nadal, B.; Bouet, C.; Patriarche, G.; Dubertret, B. Core/Shell Colloidal Semiconductor Nanoplatelets. *J. Am. Chem. Soc.* **2012**, *134*, 18591−18598.
(56) She, C.; Fedin, I.; Dolzhnikov, D. S.; Demortière, A.; Schaller, R. D.; Pelton, M.; Talapin, D. V. Low-Threshold Stimulated Emission Using Colloidal Quantum Wells. *Nano Lett.* **2014**, *14*, 2772−2777.
(57) Prudnikau, A.; Chuvilin, A.; Artemyev, M. CdSe-CdS Nanoheteroplatelets with Efficient Photoexcitation of Central CdSe Region through Epitaxially Grown CdS Wings. *J. Am. Chem. Soc.* **2013**, *135*, 14476−14479.
(58) Tessier, M. D.; Spinicelli, P.; Dupont, D.; Patriarche, G.; Ithurria, S.; Dubertret, B. Efficient Exciton Concentrators Built from Colloidal Core/Crown CdSe/CdS Semiconductor Nanoplatelets. *Nano Lett.* **2014**, *14*, 207−213.
(59) Tessier, M. D.; Mahler, B.; Nadal, B.; Heuclin, H.; Pedetti, S.; Dubertret, B. Spectroscopy of Colloidal Semiconductor Core/Shell Nanoplatelets with High Quantum Yield. *Nano Lett.* **2013**, *13*, 3321−3328.
(60) Ithurria, S.; Talapin, D. V. Colloidal Atomic Layer Deposition (c-ALD) using Self-Limiting Reactions at Nanocrystal Surface Coupled to Phase Transfer between Polar and Nonpolar Media. *J. Am. Chem. Soc.* **2012**, *134*, 18585−18590.
(61) George, S. M. Atomic Layer Deposition: An Overview. *Chem. Rev.* **2010**, *110*, 111−131.
(62) Norris, D. J.; Bawendi, M. G. Measurement and Assignment of the Size-Dependent Optical Spectrum in CdSe Quantum Dots. *Phys. Rev. B: Condens. Matter Mater. Phys.* **1996**, *53*, 16338−16346.

DOI: 10.1021/acs.jpcc.7b12629
J. Phys. Chem. C 2018, 122, 10659−10674

(63) Talapin, D. V.; Haubold, S.; Rogach, A. L.; Kornowski, A.; Haase, M.; Weller, H. A Novel Organometallic Synthesis of Highly Luminescent CdTe Nanocrystals. *J. Phys. Chem. B* **2001**, *105*, 2260−2263.
(64) Fisher, B. R.; Eisler, H.-J.; Stott, N. E.; Bawendi, M. G. Emission Intensity Dependence and Single-Exponential Behavior in Single Colloidal Quantum Dot Fluorescence Lifetimes. *J. Phys. Chem. B* **2004**, *108*, 143−148.
(65) Nirmal, M.; Dabbousi, B. O.; Bawendi, M. G.; Macklin, J. J.; Trautman, J. K.; Harris, T. D.; Brus, L. E. Fluorescence Intermittency in Single Cadmium Selenide Nanocrystals. *Nature* **1996**, *383*, 802−804.
(66) Kunneman, L. T.; Schins, J. M.; Pedetti, S.; Heuclin, H.; Grozema, F. C.; Houtepen, A. J.; Dubertret, B.; Siebbeles, L. D. A. Nature and Decay Pathways of Photoexcited States in CdSe and CdSe/CdS Nanoplatelets. *Nano Lett.* **2014**, *14*, 7039−7045.
(67) Pelton, M.; Andrews, J.; Fedin, I.; Talapin, D. V.; Leng, H.; O'Leary, S. K. Non-Monotonic Dependence of Auger Recombination Rate on Shell Thickness for CdSe/CdS Core/Shell Nanoplatelets. *Nano Lett.* **2017**, *17*, 6900−6906.
(68) Olutas, M.; Guzelturk, B.; Kelestemur, Y.; Yeltik, A.; Delikanli, S.; Demir, H. V. Lateral Size-Dependent Spontaneous and Stimulated Emission Properties in Colloidal CdSe Nanoplatelets. *ACS Nano* **2015**, *9*, 5041−5050.
(69) Yang, Z.; Pelton, M.; Fedin, I.; Talapin, D. V.; Waks, E. A Room Temperature Continuous-Wave Nanolaser Using Colloidal Quantum Wells. *Nat. Commun.* **2017**, *8*, 143.
(70) Pelton, M. Modified Spontaneous Emission in Nanophotonic Structures. *Nat. Photonics* **2015**, *9*, 427−435.
(71) Rabouw, F. T.; van der Bok, J. C.; Spinicelli, P.; Mahler, B.; Nasilowski, M.; Pedetti, S.; Dubertret, B.; Vanmaekelbergh, D. Temporary Charge Carrier Separation Dominates the Photoluminescence Decay Dynamics of Colloidal CdSe Nanoplatelets. *Nano Lett.* **2016**, *16*, 2047−2053.
(72) Pelton, M.; Ithurria, S.; Schaller, R. D.; Dolzhnikov, D. S.; Talapin, D. V. Carrier Cooling in Colloidal Quantum Wells. *Nano Lett.* **2012**, *12*, 6158−6163.
(73) Achermann, M.; Hollingsworth, J. A.; Klimov, V. I. Multiexcitons Confined Within a Subexcitonic Volume: Spectroscopic and Dynamical Signatures of Neutral and Charged Biexcitons in Ultrasmall Semiconductor Nanocrystals. *Phys. Rev. B: Condens. Matter Mater. Phys.* **2003**, *68*, 245302.
(74) Sippel, P.; Albrecht, W.; van der Bok, J. C.; Van Dijk-Moes, R. J. A.; Hannappel, T.; Eichberger, R.; Vanmaekelbergh, D. Femtosecond Cooling of Hot Electrons in CdSe Quantum-Well Platelets. *Nano Lett.* **2015**, *15*, 2409−2416.
(75) Junnarkar, M. R.; Alfano, R. R. Photogenerated High-Density Electron-Hole Plasma Energy Relaxation and Experimental Evidence for Rapid Expansion of the Electron-Hole Plasma in CdSe. *Phys. Rev. B: Condens. Matter Mater. Phys.* **1986**, *34*, 7045−7062.
(76) Yang, C. H.; Carlson-Swindle, J. M.; Lyon, S. A.; Worlock, J. M. Hot-Electron Relaxation in GaAs Quantum Wells. *Phys. Rev. Lett.* **1985**, *55*, 2359−2361.
(77) Cai, W.; Marchetti, M. C.; Lax, M. Nonequilibrium Electron-Phonon Scattering in Semiconductor Heterojunctions. *Phys. Rev. B: Condens. Matter Mater. Phys.* **1986**, *34*, 8573−8580.
(78) Vengurlekar, A. S.; Prabhu, S. S.; Roy, S. K.; Shah, J. Large Reduction in Hot-Carrier Energy-Loss Rates in CdSe Caused by Nonequilibrium Optical Phonons. *Phys. Rev. B: Condens. Matter Mater. Phys.* **1994**, *50*, 15461−15464.
(79) Baghani, E.; O'Leary, S. K.; Fedin, I.; Talapin, D. V.; Pelton, M. Auger-Limited Carrier Recombination and Relaxation in CdSe Colloidal Quantum Wells. *J. Phys. Chem. Lett.* **2015**, *6*, 1032−1036.
(80) Kunneman, L. T.; Tessier, M. D.; Heuclin, H.; Dubertret, B.; Aulin, Y. V.; Grozema, F. C.; Schins, J. M.; Siebbeles, L. D. A. Bimolecular Auger Recombination of Electron-Hole Pairs in Two-Dimensional CdSe and CdSe/CdZnS Core/Shell Nanoplatelets. *J. Phys. Chem. Lett.* **2013**, *4*, 3574−3578.
(81) Li, W.; Lian, T. Area- and Thickness-Dependent Biexciton Auger Recombination in Colloidal CdSe Nanoplatelets: Breaking the "Universal" Volume Scaling Law. *Nano Lett.* **2017**, *17*, 3152−3158.
(82) García-Santamaría, F.; Brovelli, S.; Viswanatha, R.; Hollingsworth, J. A.; Htoon, H.; Crooker, S. A.; Klimov, V. I. Breakdown of Volume Scaling in Auger Recombination in CdSe/CdS Heteronanocrystals: The Role of the Core-Shell Interface. *Nano Lett.* **2011**, *11*, 687−693.
(83) García-Santamaria, F.; Chen, Y.; Vela, J.; Schaller, R. D.; Hollingsworth, J. A.; Klimov, V. I. Suppressed Auger Recombination in "Giant" Nanocrystals Boosts Optical Gain Performance. *Nano Lett.* **2009**, *9*, 3482−3488.
(84) Park, Y.-S.; Bae, W. K.; Baker, T.; Lim, J.; Klimov, V. I. Effect of Auger Recombination on Lasing in Heterostructured Quantum Dots with Engineered Core/Shell Interfaces. *Nano Lett.* **2015**, *15*, 7319−7328.
(85) Klimov, V. I.; Ivanov, S. A.; Nanda, J.; Achermann, M.; Bezel, I.; McGuire, J. A.; Piryatinski, A. Single-Exciton Optical Gain in Semiconductor Nanocrystals. *Nature* **2007**, *447*, 441−446.
(86) Dang, C.; Lee, J.; Breen, C.; Steckel, J. S.; Coe-Sullivan, S.; Nurmikko, A. Red, Green, and Blue Lasing Enabled by Single-Exciton Gain in Colloidal Quantum Dot Films. *Nat. Nanotechnol.* **2012**, *7*, 335−339.
(87) Fan, F.; Voznyy, O.; Sabatini, R. P.; Bicanic, K. T.; Adachi, M. M.; McBride, J. R.; Reid, K. R.; Park, Y.-S.; Li, X.; Jain, A.; et al. Continuous-Wave Lasing in Colloidal Quantum Dot Solids Enabled by Facet-Selective Epitaxy. *Nature* **2017**, *544*, 75−79.
(88) Htoon, H.; Hollingworth, J. A.; Malko, A. V.; Dickerson, R.; Klimov, V. I. Light Amplification in Semiconductor Nanocrystals: Quantum Rods Versus Quantum Dots. *Appl. Phys. Lett.* **2003**, *82*, 4776−4778.
(89) Shaklee, K. L.; Leheny, R. F. Direct Determination of Optical Gain in Semiconductor Crystals. *Appl. Phys. Lett.* **1971**, *18*, 475−477.
(90) Tessier, M. D.; Biadala, L.; Bouet, C.; Ithurria, S.; Abecassis, B.; Dubertret, B. Phonon Line Emission Revealed by Self-Assembly of Colloidal Nanoplatelets. *ACS Nano* **2013**, *7*, 3332−3340.
(91) Guzelturk, B.; Erdem, O.; Olutas, M.; Kelestemur, Y.; Demir, H. V. Stacking in Colloidal Nanoplatelets: Tuning Excitonic Properties. *ACS Nano* **2014**, *8*, 12524−12533.
(92) Xia, R.; Heliotis, G.; Bradley, D. D. C. Fluorene-Based Polymer Gain Media for Solid-State Laser Emission Across the Full Visible Spectrum. *Appl. Phys. Lett.* **2003**, *82*, 3599−3601.
(93) Xing, G.; Mathews, N.; Lim, S. S.; Yantara, N.; Liu, X.; Sabba, D.; Grätzel, M.; Mhaisalkar, S.; Sum, T. C. Low-Temperature Solution-Processed Wavelength-Tunable Perovskites for Lasing. *Nat. Mater.* **2014**, *13*, 476−480.
(94) Guzelturk, B.; Kelestemur, Y.; Olutas, M.; Delikanli, S.; Demir, H. V. Amplified Spontaneous Emission and Lasing in Colloidal Nanoplatelets. *ACS Nano* **2014**, *8*, 6599−6605.
(95) Li, Q.; Xu, Z.; McBride, J. R.; Lian, T. Low Threshold Multiexciton Optical Gain in Colloidal CdSe/CdTe Core/Crown Type-II Nanoplatelet Heterostructures. *ACS Nano* **2017**, *11*, 2545−2533.
(96) Chan, Y.; Caruge, J.-M.; Snee, P. T.; Bawendi, M. G. Multiexcitonic Two-State Lasing in a CdSe Nanocrystal Laser. *Appl. Phys. Lett.* **2004**, *85*, 2460−2462.
(97) She, C.; Fedin, I.; Dolzhnikov, D. S.; Dahlberg, P. D.; Engel, G. S.; Schaller, R. D.; Talapin, D. V. Red, Yellow, Green, and Blue Amplified Spontaneous Emission and Lasing Using Colloidal CdSe Nanoplatelets. *ACS Nano* **2015**, *9*, 9475−9485.
(98) Kelestemur, Y.; Dede, D.; Gungor, K.; Usanmaz, C. F.; Erdem, O.; Demir, H. V. Alloyed Heterostructures of $CdSe_xS_{1-x}$ with Highly Tunable Optical Gain Performance. *Chem. Mater.* **2017**, *29*, 4857−4865.
(99) Diroll, B. T.; Talapin, D. V.; Schaller, R. D. Violet-to-Blue Gain and Lasing from Colloidal CdS Nanoplatelets: Low-Threshold Stimulated Emission Despite Low Photoluminescence Quantum Yield. *ACS Photonics* **2017**, *4*, 576−583.

DOI: 10.1021/acs.jpcc.7b12629
J. Phys. Chem. C 2018, 122, 10659−10674

(100) Li, M.; Zhi, M.; Zhu, H.; Wu, W.-Y.; Xu, Q.-H.; Jhon, M. H.; Chan, Y. Ultralow-Threshold Multiphoton-Pumped Lasing from Colloidal Nanoplatelets in Solution. *Nat. Commun.* **2015**, *6*, 8513.
(101) Grim, J. Q.; Christodoulou, S.; Di Stasio, F.; Krahne, R.; Cingolani, R.; Manna, L.; Moreels, I. Continuous-Wave Biexciton Lasing at Room Temperature Using Solution-Processed Quantum Wells. *Nat. Nanotechnol.* **2014**, *9*, 891−895.
(102) Pelton, M.; Bryant, G. W. *Introduction to Metal-Nanoparticle Plasmonics*; John Wiley & Sons, Hoboken, NJ, 2013.
(103) Khurgin, J. B. How to Deal with the Loss in Plasmonics and Metamaterials. *Nat. Nanotechnol.* **2015**, *10*, 2−6.
(104) Akahane, Y.; Asano, T.; Song, B.-S.; Noda, S. High-Q Photonic Nanocavity in a Two-Dimensional Photonic Crystal. *Nature* **2003**, *425*, 944−947.
(105) Joannopoulos, J. D.; Johnson, S. G.; Winn, J. N.; Meade, R. D. *Photonic Crystals: Molding the Flow of Light*, 2nd ed.; Princeton University Press, Princeton, NJ, 2008.
(106) Khan, M.; Babinec, T.; McCutcheon, M. W.; Deotare, P.; Lončar, M. Fabrication and Characterization of High-Quality-Factor Silicon Nitride Nanobeam Cavities. *Opt. Lett.* **2011**, *36*, 421−423.
(107) Björk, G.; Yamamoto, Y. Analysis of Semiconductor Microcavity Lasers Using Rate Equations. *IEEE J. Quantum Electron.* **1991**, *27*, 2386−2396.
(108) Björk, G.; Karlsson, A.; Yamamoto, Y. Definition of a Laser Threshold. *Phys. Rev. A: At., Mol., Opt. Phys.* **1994**, *50*, 1675−1680.
(109) Björk, G.; Karlsson, A.; Yamamoto, Y. On the Linewidth of Microcavity Lasers. *Appl. Phys. Lett.* **1992**, *60*, 304−306.
(110) Huang, J.; Kim, S.-H.; Gardner, J.; Regreny, P.; Seassal, C.; Aitor Postigo, P.; Scherer, A. Room Temperature, Continuous-Wave Coupled-Cavity InAsP/InP Photonic Crystal Laser with Enhanced Far-Field Emission Directionality. *Appl. Phys. Lett.* **2011**, *99*, 091110.
(111) Jang, H.; Karnadi, I.; Pramudita, P.; Song, J.-H.; Soo Kim, K.; Lee, Y.-H. Sub-microWatt Threshold Nanoisland Lasers. *Nat. Commun.* **2015**, *6*, 8276.
(112) Quan, Q.; Deotare, P. B.; Lončar, M. Photonic Crystal Nanobeam Cavity Strongly Coupled to the Feeding Waveguide. *Appl. Phys. Lett.* **2010**, *96*, 203102.
(113) Miller, D. A. B. Device Requirements for Optical Interconnects to Silicon Chips. *Proc. IEEE* **2009**, *97*, 1166−1185.
(114) Lin, C. H.; Lafalce, E.; Jung, J.; Smith, M. J.; Malak, S. T.; Aryal, S.; Yoon, Y. J.; Zhai, Y.; Lin, Z.; Vardeny, Z. V.; et al. Core/Alloyed-Shell Quantum Dot Robust Solid Films with High Optical Gains. *ACS Photonics* **2016**, *3*, 647−658.
(115) Anikeeva, P. O.; Madigan, C. F.; Halpert, J. E.; Bawendi, M. G.; Bulović, V. Electronic and Excitonic Processes in Light-Emitting Devices Based on Organic Materials and Colloidal Quantum Dots. *Phys. Rev. B: Condens. Matter Mater. Phys.* **2008**, *78*, 085434.
(116) Bae, W. K.; Park, Y.-S.; Lim, J.; Lee, D.; Padilha, L. A.; McDaniel, H.; Robel, I.; Lee, C.; Pietryga, J. M.; Klimov, V. I. Controlling the Influence of Auger Recombination on the Performance of Quantum-Dot Light-Emitting Diodes. *Nat. Commun.* **2013**, *4*, 2661.
(117) Rowland, C. E.; Fedin, I.; Zhang, H.; Gray, S. K.; Govorov, A. O.; Talapin, D. V.; Schaller, R. D. Picosecond Energy Transfer and Multiexciton Transfer outpaces Auger Recombination in Binary CdSe Nanoplatelet Solids. *Nat. Mater.* **2015**, *14*, 484−489.
(118) Berggren, M.; Dodabalapur, A.; Slusher, R. E.; Bao, Z. Light Amplification in Organic Thin Films Using Cascade Energy Transfer. *Nature* **1997**, *389*, 466−469.
(119) Bradshaw, L. R.; Knowles, K. E.; McDowall, S.; Gamelin, D. R. Nanocrystals for Luminescent Solar Concentrators. *Nano Lett.* **2015**, *15*, 1315−1323.
(120) Sharma, M.; Gungor, K.; Yeltik, A.; Olutas, M.; Guzelturk, B.; Kelestemur, Y.; Erdem, T.; Delikanli, S.; McBride, J. R.; Demir, H. V. Near-Unity Emitting Copper-Doped Colloidal Semiconductor Quantum Wells for Luminescent Solar Concentrators. *Adv. Mater.* **2017**, *29*, 1700821.
(121) Vaxenburg, R.; Rodina, A.; Lifshitz, E.; Efros, A. L. Biexciton Auger Recombination in CdSe/CdS Core/Shell Semiconductor Nanocrystals. *Nano Lett.* **2016**, *16*, 2503−2511.
(122) Jain, A.; Voznyy, O.; Hoogland, S.; Korkusinski, M.; Hawrylak, P.; Sargent, E. H. Atomistic Design of CdSe/CdS Core-Shell Quantum Dots with Suppressed Auger Recombination. *Nano Lett.* **2016**, *16*, 6491−6496.
(123) Cragg, G. E.; Efros, A. L. Suppression of Auger Processes in Confined Structures. *Nano Lett.* **2010**, *10*, 313−317.
(124) Nasilowski, M.; Spinicelli, P.; Patriarche, G.; Dubertret, B. Gradient CdSe/CdS Quantum Dots with Room Temperature Biexciton Unity Quantum Yield. *Nano Lett.* **2015**, *15*, 3953−3958.
(125) Park, Y.-S.; Lim, J.; Makarov, N. S.; Klimov, V. I. Effect of Interfacial Alloying versus "Volume Scaling" on Auger Recombination in Compositionally Graded Semiconductor Quantum Dots. *Nano Lett.* **2017**, *17*, 5607−5613.
(126) Qin, W.; Liu, H.; Guyot-Sionnest, P. Small Bright Charged Colloidal Quantum Dots. *ACS Nano* **2014**, *8*, 283−291.
(127) Pedetti, S.; Ithurria, S.; Heuclin, H.; Patriarche, G.; Dubertret, B. Type-II CdSe/CdTe Core/Crown Semiconductor Nanoplatelets. *J. Am. Chem. Soc.* **2014**, *136*, 16430−16438.
(128) Guzelturk, B.; Kelestemur, Y.; Olutas, M.; Li, Q.; Lian, T.; Demir, H. V. High-Efficiency Optical Gain in Type-II Semiconductor Nanocrystals of Alloyed Colloidal Quantum Wells. *J. Phys. Chem. Lett.* **2017**, *8*, 5317−5324.
(129) Golub, J. E.; Kash, K.; Harbison, J. P.; Florez, L. T. Long-Lived Spatially Indirect Excitons in Coupled GaAs/$Al_xGa_{1-x}As$ Quantum Wells. *Phys. Rev. B: Condens. Matter Mater. Phys.* **1990**, *41*, 8564−8467.
(130) Alexandrou, A.; Kash, J. A.; Mendez, E. E.; Zachau, M.; Hong, J. M.; Fukuzawa, T.; Hase, Y. Electric-Field Effects on Exciton Lifetimes in Symmetric Coupled GaAs/$Al_{0.3}Ga_{0.7}As$ Double Quantum Wells. *Phys. Rev. B: Condens. Matter Mater. Phys.* **1990**, *42*, 9225−9228.
(131) Bouet, C.; Laufer, D.; Mahler, B.; Nadal, B.; Heuclin, H.; Pedetti, S.; Patriarche, G.; Dubertret, B. Synthesis of Zinc and Lead Chalcogenide Core and Core/Shell Nanoplatelets Using Sequential Cation Exchange Reactions. *Chem. Mater.* **2014**, *26*, 3002−3008.
(132) Riedinger, A.; Ott, F. D.; Mule, A.; Mazzotti, S.; Knüsel, P. N.; Kress, S. J. P.; Prins, F.; Erwin, S. C.; Norris, D. J. An Intrinsic Growth Instability in Isotropic Materials Leads to Quasi-Two-Dimensional Nanoplatelets. *Nat. Mater.* **2017**, *16*, 743−748.
(133) Cao, Y. C. Synthesis of Square Gadolinium-Oxide Nanoplates. *J. Am. Chem. Soc.* **2004**, *126*, 7456−7457.
(134) Zhang, Y.-W.; Sun, X.; Si, R.; You, L.-P.; Yan, C.-H. Single-Crystalline and Monodisperse LaF_3 Triangular Nanoplates from a Single-Source Precursor. *J. Am. Chem. Soc.* **2005**, *127*, 3260−3261.
(135) Park, K. H.; Jang, K.; Son, S. U. Synthesis, Optical Properties, and Self-Assembly of Ultrathin Hexagonal In_2S_3 Nanoplates. *Angew. Chem., Int. Ed.* **2006**, *45*, 4608−4612.
(136) Huo, Z.; Tsung, C.-K.; Huang, W.; Fardy, M.; Yan, R.; Zhang, X.; Li, Y.; Yang, P. Self-Organized Ultrathin Oxide Nanocrystals. *Nano Lett.* **2009**, *9*, 1260−1264.
(137) Vaughn, D. D., II; Patel, R. J.; Hickner, M. A.; Schaak, R. E. Single-Crystal Colloidal Nanosheets of GeS and GeSe. *J. Am. Chem. Soc.* **2010**, *132*, 15170−15172.
(138) Jang, J.-T.; Jeong, S.; Seo, J.-W.; Kim, M.-C.; Sim, E.; Oh, Y.; Nam, S.; Park, B.; Cheon, J. Ultrathin Zirconium Disulfide Nanodiscs. *J. Am. Chem. Soc.* **2011**, *133*, 7636−7639.
(139) Jeong, S.; Yoo, D.; Jang, J. T.; Kim, M.; Cheon, J. Well-Defined Colloidal 2-D Layered Transition-Metal Chalcogenide Nanocrystals via Generalized Synthetic Protocols. *J. Am. Chem. Soc.* **2012**, *134*, 18233−18236.
(140) Jung, W.; Lee, S.; Yoo, D.; Jeong, S.; Miró, P.; Kuc, A.; Heine, T.; Cheon, J. Colloidal Synthesis of Single-Layer MSe_2 (M = Mo, W) Nanosheets via Anisotropic Solution-Phase Growth Approach. *J. Am. Chem. Soc.* **2015**, *137*, 7266−7269.
(141) Tyagi, P.; Arveson, S. M.; Tisdale, W. A. Colloidal Organohalide Perovskite Nanoplatelets Exhibiting Quantum Confinement. *J. Phys. Chem. Lett.* **2015**, *6*, 1911−1916.

DOI: 10.1021/acs.jpcc.7b12629
J. Phys. Chem. C 2018, 122, 10659−10674

(142) Bekenstein, Y.; Koscher, B. A.; Eaton, S. W.; Yang, P.; Alivisatos, A. P. Highly Luminescent Colloidal Nanoplatelets of Perovskite Cesium Lead Halide and Their Oriented Assemblies. *J. Am. Chem. Soc.* **2015**, *137*, 16008−16011.
(143) Akkerman, Q. A.; Motti, S. G.; Srimath Kandada, A. R.; Mosconi, E.; D'Innocenzo, V.; Bertoni, G.; Marras, S.; Kamino, B. A.; Miranda, L.; De Angelis, F.; et al. Solution Synthesis Approach to Colloidal Cesium Lead Halide Perovskite Nanoplatelets with Monolayer-Level Thickness Control. *J. Am. Chem. Soc.* **2016**, *138*, 1010−1016.
(144) Novoselov, K. S.; Mishchenko, A.; Carvalho, A.; Castro Neto, A. H. 2D Materials and van der Waals Heterostructures. *Science* **2016**, *353*, aac9439.

DOI: 10.1021/acs.jpcc.7b12629
J. Phys. Chem. C 2018, 122, 10659−10674